Geologia USP
Série Científica

DOI: 10.5327/Z1519-874X2013000100005

Revista do Instituto de Geociências - USP

Geol. USP, Sér. cient., São Paulo, v. 13, n. 1, p. 73-94, Março 2013

Tourmalinites of the Brusque Group in the São João Batista-Tijucas area, State of Santa Catarina, Brazil

Turmalinitos do Grupo Brusque na região entre São João Batista e Tijucas, Santa Catarina, Brasil

Gianna Maria Garda[1], Fabio Brentan[1], Miguel Angelo Stipp Basei[1]

[1]Departamento de Mineralogia e Geotectônica, Instituto de Geociências, Universidade de São Paulo - USP, Rua do Lago, 562, CEP 05508-080, São Paulo, SP, BR (giagarda@usp.br; fabio.brentan@usp.br; baseimas@usp.br)

Received 08 August 2012; accepted 07 November 2012

Abstract

The Dom Feliciano Belt, in the State of Santa Catarina, is represented by the Itajaí and Brusque groups and the Florianópolis Batholith. The basal Rio do Oliveira Formation of the Brusque Group consists of metabasic/calc-silicate, metavolcanic-exhalative, metapelitic and metapsammitic units. A discontinuous tourmalinite sequence integrating the metavolcanic-exhalative unit stretches out from São João Batista to Tijucas. Two types of tourmalinites were distinguished and named Rio do Oliveira and Morro do Carneiro. The first is very fine-grained, banded, and composed of greenish-yellow or brown tourmaline. The second is coarser-grained, massive to slightly foliated, and composed of color-zoned tourmaline. Microprobe and laser ablation-ICPMS analyses showed that the Rio do Oliveira tourmaline is richer in Al, alkalis, and poorer in Ti, Mg, Fe and Ca when compared to the Morro do Carneiro tourmaline. Rio do Oliveira tourmalinites were formed by selective substitution of pelitic and psammitic sediments by percolation of B-rich fluids through the volcanic-sedimentary unit during diagenesis and metamorphism. Morro do Carneiro tourmaline has detrital cores and rims enriched in Mg, Fe, Ti, Mn, Sr, Co and Ca, when compared to the Rio do Oliveira tourmaline. An intermediate dark zone is Ti- and Fe-rich. The abrupt increase in Ca from core to rim may have resulted from the equilibrium with the surrounding Ca-rich environment (underlying calc-silicate rocks). Even if the REE patterns obtained for Rio do Oliveira and Morro do Carneiro tourmalines are practically identical, it is proposed that the fluids that generated the Morro do Carneiro tourmalinites have also been metasomatic/igneous.

Keywords: Dom Feliciano Belt; Brusque Group; Tourmalinites.

Resumo

O Cinturão Dom Feliciano no Estado de Santa Catarina é representado pelos grupos Itajaí e Brusque e o Batólito Florianópolis. A Formação Rio do Oliveira, basal do Grupo Brusque, constitui-se de unidades metabásicas/cálcio-silicáticas, metavulcânicas-exalativas, metapelíticas e metapsamíticas. Uma sequência descontínua de turmalinitos integrante da unidade metavulcânica-exalativa estende-se desde São João Batista até Tijucas. Dois tipos de turmalinitos foram distintos e denominados Rio do Oliveira e Morro do Carneiro. O primeiro é muito fino, bandado e composto por turmalina amarela-esverdeada ou castanha. O segundo é mais grosso, de textura maciça a levemente foliada, e formado por turmalina zonada. Análises por microssonda eletrônica e *laser ablation*-ICPMS mostraram que a turmalina do Rio do Oliveira é mais rica em Al, álcalis e mais pobre em Ti, Mg, Fe and Ca quando comparada com a do Morro do Carneiro. Os turmalinitos do Rio do Oliveira formaram-se por substituição seletiva de sedimentos pelíticos e psammíticos resultante da percolação de fluidos ricos em boro pela unidade vulcano-sedimentar durante a diagênese e metamorfismo. A turmalina do Morro do Carneiro possui núcleos detríticos e bordas mais ricas em Mg, Fe, Ti, Mn, Sr, Co e Ca que a turmalina do Rio do Oliveira. Uma zona intermediária escura é mais rica em Ti e Fe. O aumento brusco em Ca do núcleo para a borda pode ter resultado do equilíbrio com o ambiente circunvizinho rico em Ca (rochas cálcio-silicáticas subjacentes). Mesmo que os padrões definidos pelos ETR para as turmalinas do Rio do Oliveira e do Morro do Carneiro sejam praticamente idênticos, propõe-se que os fluidos formadores do turmalinito do Morro do Carneiro possam também ter tido origem metassomática/ígnea.

Palavras-chave: Cinturão Dom Feliciano; Grupo Brusque; Turmalinitos.

INTRODUCTION

The Brusque Group tourmalinites are distributed along a 10 km-long belt, from São João Batista to Tijucas, in eastern Santa Catarina. They crop out as meter-sized blocks and boulders and tabular lenses associated with quartzites, garnet-muscovite schists, amphibolites, metatuffs and calc-silicate rocks that compose the metavolcanosedimentary sequence of the Rio do Oliveira Formation. Despite being discontinuous, the Brusque Group tourmalinites are one of the most extensive ever described in literature (e.g., Silva et al., 1985; Basei, Campos Neto, Siga Jr, 1994).

Brentan (2011) compiled a geological map for the region of São João Batista-Tijucas on the basis of field work carried out by Geology students during the Geological Mapping courses of 1992 (Tijucas), 2003 (São João Batista) and 2008 (Itapema). Focusing on tourmalinite occurrences, Brentan (2011) carried out petrography and mineral analyses of tourmalines and amphiboles of tourmalinites and underlying amphibolites using the electron microprobe. Brentan's (2011) study helped characterize two types of tourmalinites, which were informally named Rio do Oliveira and Morro do Carneiro. Additionally, zircon separates from schist, calc-silicate and metabasic rocks associated with tourmalinites were dated by the U-Pb LA-ICPMS method in order to constrain the ages of tourmalinite formation.

As a follow-up to Brentan's (2011) research, this paper presents new trace-element data on the tourmalines of Rio do Oliveira and Morro do Carneiro tourmalinites, as a contribution to the understanding of the generation of these rocks.

REGIONAL GEOLOGY

Dom Feliciano Belt, the main geotectonic unit of the southern portion of the Mantiqueira Province, is a N-S trending belt approximately 1,200 km long and 150 km wide, which stretches out from southern Brazil to Uruguay (Basei, 1985). It resulted from successive subduction and collision events that occurred during the Neoproterozoic and that compose the tectono-magmatic events associated with the formation of Western Gondwana (Basei, 2000). Three crustal segments constitute the Dom Feliciano Belt: the Granitoid Belt, the Metavolcanosedimentary Belt (which comprises the Brusque Group to the north, and the Porongos and Lavalleja groups to the south), and the Foreland Basins. The Major Gercino Shear Zone separates the Granitoid Belt from the Metavolcanosedimentary Belt, and low-angle faults separate the Metavolcanosedimentary Belt from the Foreland Basins, placing the Brusque Group on the Itajaí Basin sediments (Basei et al., 2000, 2011).

The northern portion of Dom Feliciano Belt in Santa Catarina is presented in Figure 1. The granitoids that occur south to the Major Gercino Shear Zone represent magmatic arc roots and constitute the Southeastern Domain of the Dom Feliciano Belt; the Brusque Group metasediments and the associated volcanic rocks belong to the Central Domain, and the Itajaí Basin sediments and the felsic igneous rocks compose the Northwestern Domain.

THE BRUSQUE GROUP

The Brusque Group stretches out for *ca*. 75 km, from Itajaí southwestwards to Vidal Ramos, where it is covered by the Paraná Basin. It is up to 45 km wide, and is divided in two parts by the Valsungana batholith (Silva, 1991). The Major Gercino Shear Zone marks its southern limit with granitic-migmatitic terrains. The northern limit is marked by the contact with the São Miguel Complex. To NW it thrusts over the Itajaí Basin sediments.

Silva (1991) divided the previously named Brusque Metamorphic Complex into three metavolcanosedimentary sequences: Ribeirão do Cinema, Ribeirão do Ouro and Rio do Oliveira-Itapema, the latter including tourmalinite occurrences. Other characteristics used by the author to distinguish Ribeirão do Ouro and Rio do Oliveira-Itapema sequences were the distribution of chemical-exhalative associations, the occurrence of basaltic flows with variolitic structure and locally pillow lavas, felsic graywackes, limestones, dolomites and rhythmic rocks with turbiditic affinity, present in the Ribeirão do Ouro Sequence and lacking in the Rio do Oliveira-Itapema Sequence. The metamorphism in the Rio do Oliveira-Itapema Sequence reaches high greenschist – low amphibolite facies, whereas in the Ribeirão do Ouro Sequence it is restricted to the low greenschist facies.

Philipp et al. (2004) divided the Brusque Group into five sub-units (Clastic, Chemical, Clastic-Chemical, Basic Metavolcanic and Magnesian) on the basis of dominant protoliths. The tourmalinites were included in the Clastic Sub-unit, concordantly intercalated in the metapelites as 2 to 4 m-thick lenses.

Basei et al. (2011) separated the Brusque Group from top to bottom into the Rio da Areia, Botuverá and Rio do Oliveira Formations. The Rio do Oliveira and Rio da Areia Formations comprise metavolcanosedimentary rocks, whereas the Botuverá Formation comprises metasedimentary rocks.

The Rio do Oliveira Formation is the main metavolcanosedimentary unit of the Brusque Group and is located south to the Valsungana batholith, close to Tijucas. It is composed from top to bottom of metapsammites, metapelites, a metavolcano-exhalative sequence and basic

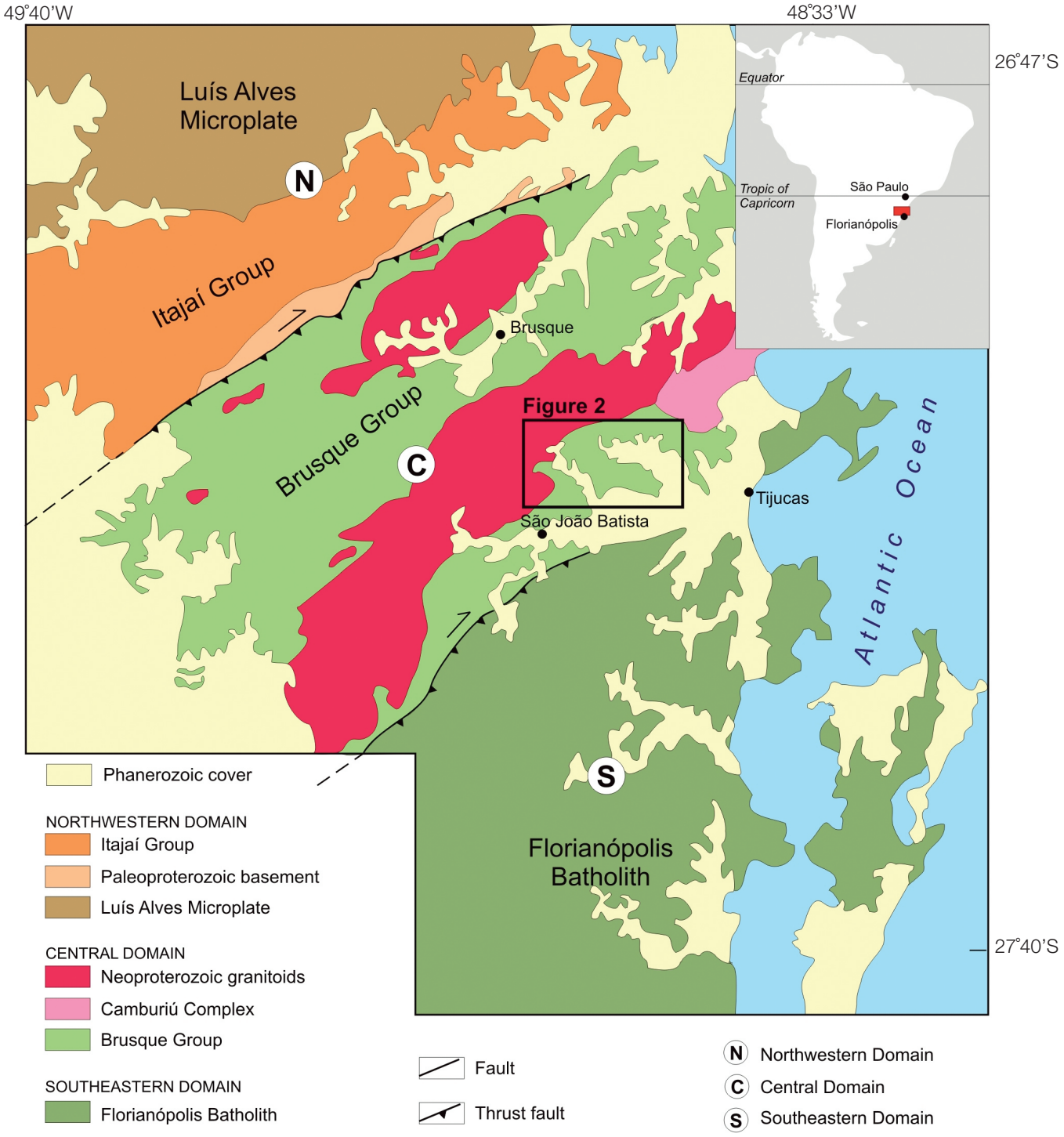

Figure 1. The Brusque Group in the tectonic context of the Dom Feliciano Belt in Santa Catarina (modified after Basei et al., 2011).

metavolcanic and calc-silicate rocks. It is overthrusted by the Botuverá Formation to the south, and is in contact with the Valsungana Granite to the north (Figure 2).

The metapsammitic unit is located on top of the Rio do Oliveira Formation and is best exposed in Morro do Carneiro (point 2 of Figure 2). It is composed of homogeneous, gray, massive orthoquartzites at the base that grade to thinly banded meta-rhythmites with bands constituted of quartzite and sericite-quartz schist. On the top, a polymictic metaconglomerate occurs and is composed of a fine-grained sandy matrix and clasts that vary from 1 to 20 cm in size. Dark gray millimeter-sized bands composed of quartzites and hematite-rich bands containing porphyroblastic magnetite may represent BIFs (Basei et al., 2011).

In the metapelitic unit mica schists predominate, composed of quartz-muscovite schists containing garnet, biotite and porphyroblastic andalusite; sericite-quartz schist containing biotite, and quartz-muscovite schist containing garnet and graphite. Amphibolite, garnet amphibolite, quartzite and garnet-bearing calc-silicate intercalations are common (Basei et al., 2011).

Tourmalinites, tourmaline-rich quartzites and more rarely carbonatic rocks constitute the metavolcanic-exhalative unit. Close to the contact with the Valsungana Granite, a metapelitic intercalation is observed, composed of greenish gray sillimanite-quartz-mica schist locally containing andalusite and cordierite generated by contact metamorphism (Basei et al., 2011).

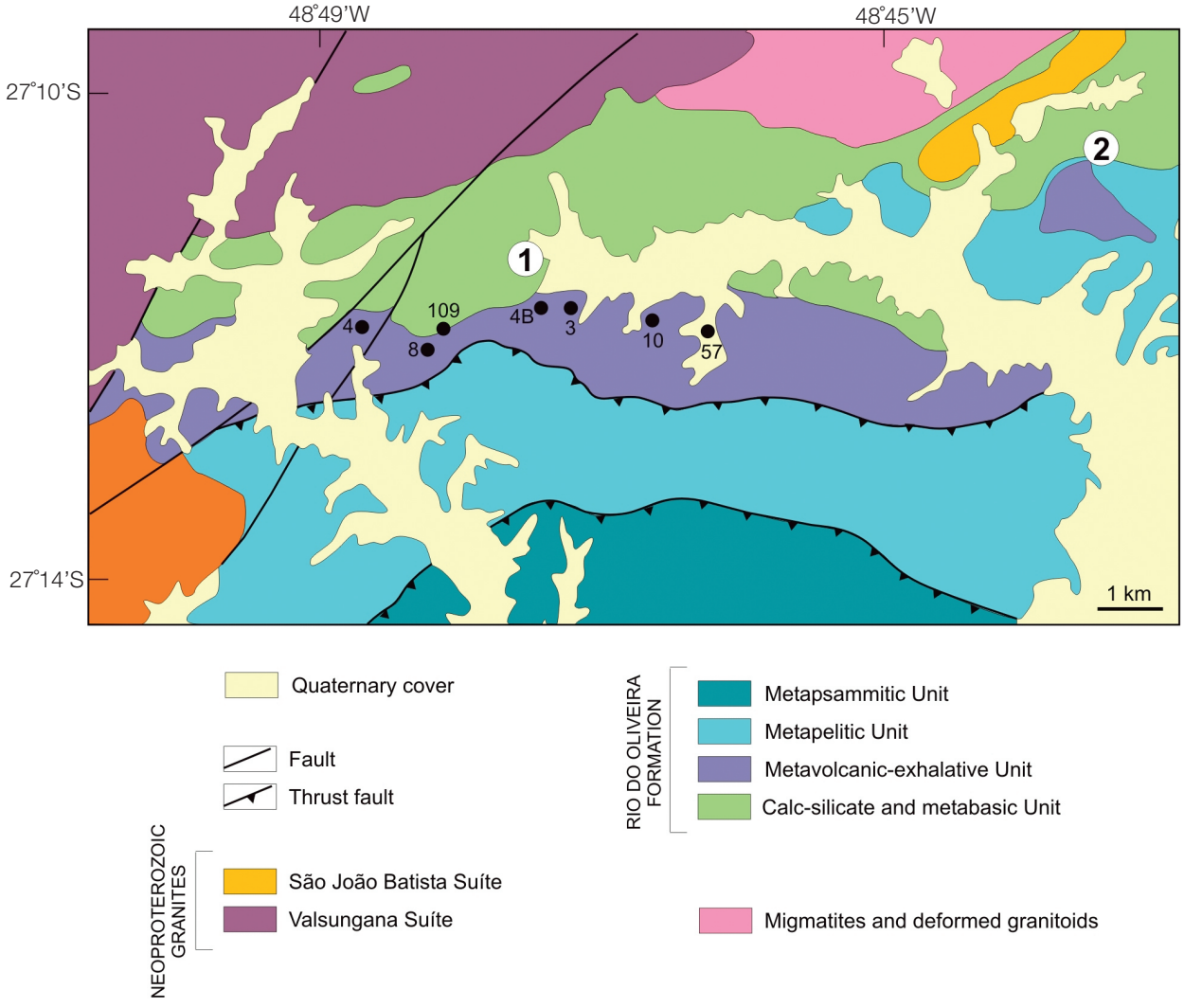

Figure 2. Geologic map of the São João Batista-Tijucas region (after Brentan, 2011). Point 1: Rio do Oliveira tourmalinite (IT-VI-42a); point 2: Morro do Carneiro tourmalinite (IT-VII-39). Numbered black circles refer to outcrops of the Rio do Oliveira-type tourmalinites.

The metabasic rocks and other rocks of the metavolcanic-exhalative sequence subjacent to the tourmalinites are represented by fine- to medium-grained, greenish dark-gray amphibolites showing millimeter-sized banding. They are composed of plagioclase, opaque minerals, hornblende, actinolite and subordinated zircon and epidote. The protolith corresponds to carbonatic rocks, basic tuffs and more rarely ultramafites. Variations in the deformation and metamorphism intensity are observed, thus predominating the nematoblastic texture with granoblastic portions and relict igneous textures. Blastoporphyritic and blastoamygdaloidal textures are less frequent.

Calc-silicate rocks (andesine-chlorite-sericite-epidote-quartz gneiss and quartz-chlorite-andesine-actinolite gneiss) were generated from carbonatic rocks and basic tuffs. Relict banding is evidenced by granoblastic (carbonatic) bands and nematoblastic, mafic (amphibolitic) bands. Andesine, actinolite, tremolite, epidote, chlorite and clinozoisite are common and opaque minerals are accessories. Metatuffs correspond to greenish-gray banded rocks, with lighter bands composed of plagioclase and subordinated quartz and darker bands composed of hornblende. The presence of muscovite in some bands indicate siliciclastic sedimentary influence (Basei et al., 2011). Albite, titanite, epidote, diopside (altered to hornblende) are accessories.

The tourmalinites of the Brusque Group

The tourmalinites of the Brusque Group are composed of millimeter-sized quartz (chert) and tourmaline bands. They are dark gray, sometimes stained by iron and manganese oxides. Under the microscope they are fine-grained and show granonematoblastic texture with serrated contacts between quartz, tourmaline, pyrite and magnetite. Common accessories are amphibole, zircon, monazite and chlorite.

The tourmalinites, informally named Rio do Oliveira, crop out as blocks and boulders of alternating millimeter-sized whitish quartz (chert) bands and dark-gray tourmaline bands (point 1 of Figures 2 and 3A). The compositional banding is parallel to main foliation S2, which sometimes is folded and crenulated (Figure 3B). This banding is very regular, but in some places the tourmaline bands become thicker, reaching

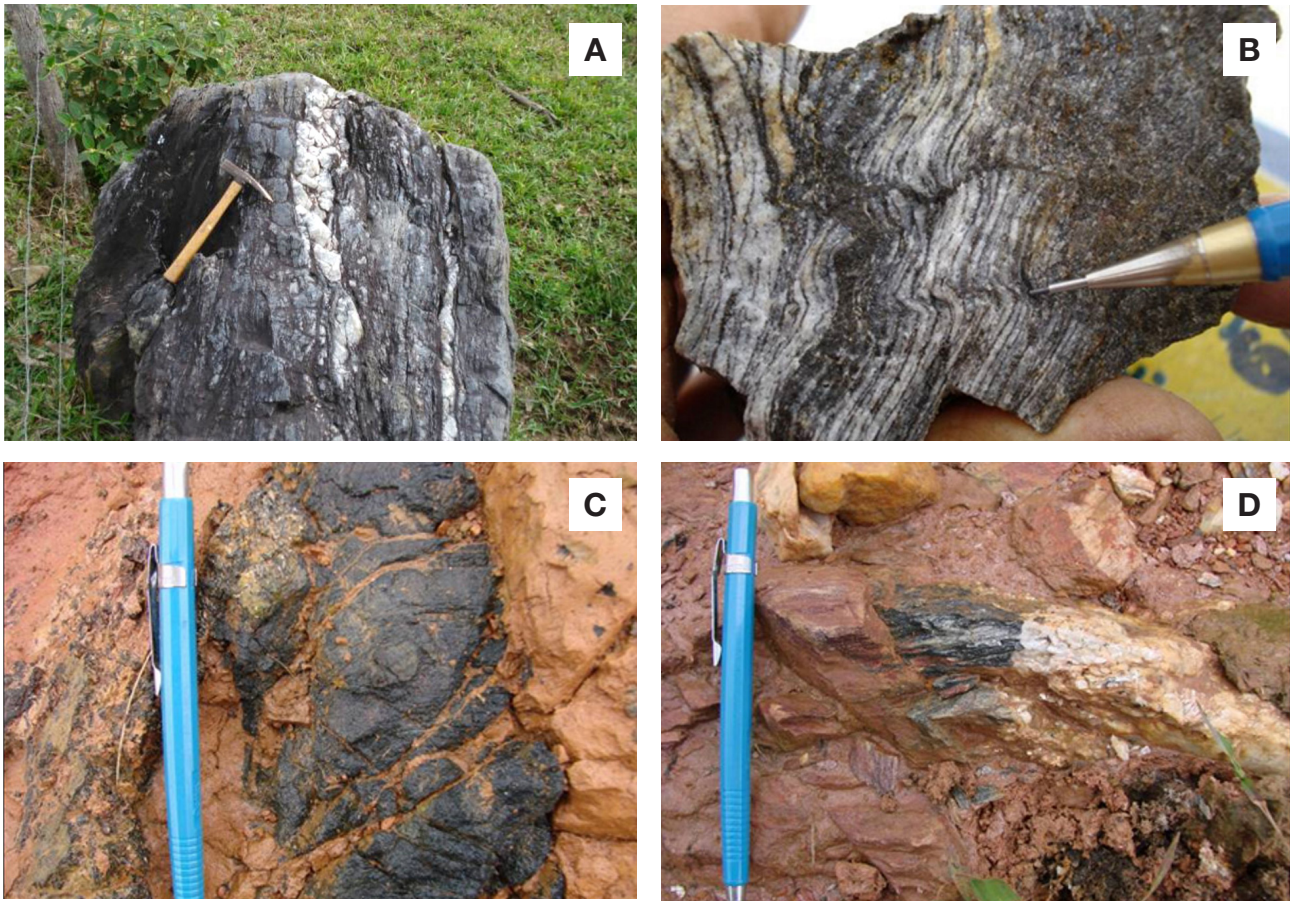

Figure 3. Tourmalinite crops out as: (A) blocks and boulders; (B) crenulated tourmalinite with tourmaline-rich veins truncating the foliation; (C) massive band of very tourmaline-rich tourmalinite intercalated with altered sericite schist, and (D) muscovite-rich pegmatitic vein truncating the tourmalinite.

more than 50 cm. They can even form masses essentially composed of tourmaline (Figure 3C). These masses are more common close to tourmaline-rich veins that truncate banding. Another type of tourmalinite occurs NW to the Morro do Carneiro (point 2 of Figure 2) as massive lenses up to 1 m-thick, intercalated with muscovite-quartz schist and amphibolites, and crosscut by muscovite-rich pegmatite veins (Figure 3D).

Under the microscope, the texture of the banded Rio do Oliveira tourmalinites is predominantly nematoblastic, generated by tourmaline prisms oriented along the foliation and occasionally by actinolite/hornblende (Figure 4A). The granoblastic texture is defined by quartz with undulating extinction, the contact between the grains being serrate to lobate and recrystallized at the rims (Figure 4B). In the tourmaline-rich bands the occurrence of plagioclase associated with actinolite is common. The brown tourmaline is very fine-grained (*ca*. 0.2-mm long, 0.05 mm-diameter basal section, Figure 4C) and may be colored-zoned. In contrast, the tourmaline of Morro do Carneiro tourmalinites is usually color-zoned, with bluish cores and greenish rims when finer-grained, and with a light-green core, a dark intermediate zone and an olive-green rim, when coarser-grained (Figure 4D). The diameter of the basal section varies from *ca*. 64 mm to 0.2 mm. The Morro do Carneiro tourmaline may overgrow other tourmaline and even quartz grains.

Geochronology

According to Basei et al. (2011), recent U-Pb geochronological studies by SHRIMP have undoubtedly confirmed that the Brusque Group deposition, metamorphism and magmatism occurred during the Ediacaran.

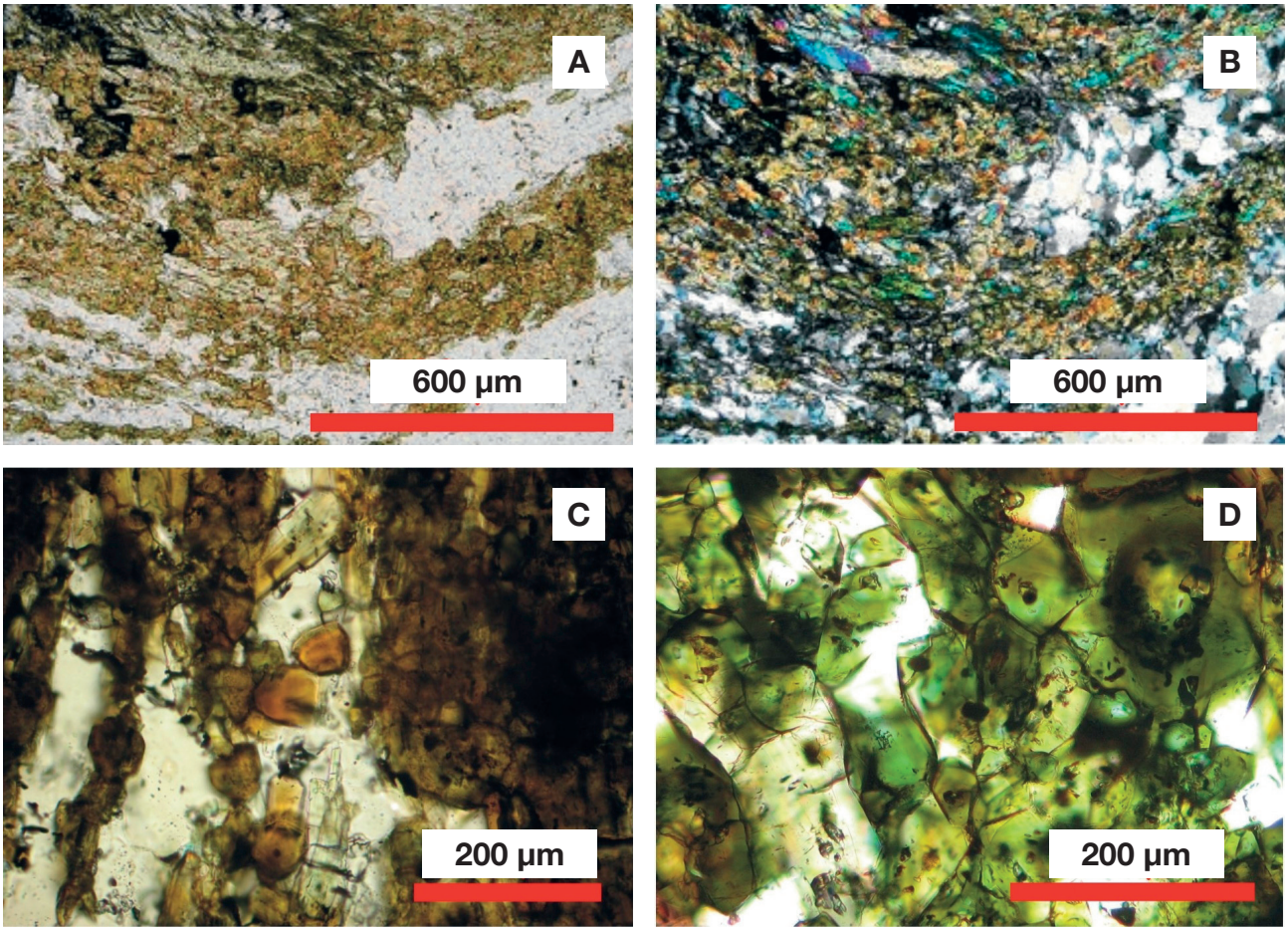

Figure 4. (A) Banded Rio do Oliveira tourmalinite containing fibrous, greenish amphibole (top left side of the photomicrograph). Brownish tourmaline-rich bands alternate with whitish quartz-rich bands (plane-polarized light). (B) Same as A under crossed nicols, evidencing quartz recrystallization with lobate contacts (sample IT-VI-04b). (C) Brown, weakly zoned tourmaline (sample IT-VI-42a, plane-polarized light). (D) Coarser-grained, Morro do Carneiro zoned tourmaline (top right), with light-green core, an intermediate dark zone, and an olive-green rim. Smaller tourmaline crystals have bluish cores and greenish rims (sample IT-VII-39, plane-polarized light).

The age of 936 ± 40 Ma obtained for a metagabbro (Yamamoto, 2010; Basei et al., 2011) marks the beginning of the taphrogeny that originated the Brusque paleobasin. The youngest ages of 552.0 ± 3.4 Ma obtained for the Brusque granitoids by K-Ar dating (Basei et al., 2011) represent a late regional tectono-thermal episode affecting the metasedimentary and metavolcanic rocks. In contrast to the Neoproterozoic ages that establish the evolution of the Brusque Group, detrital zircon ages (Hartmann et al., 2003; Basei et al., 2008) indicate as preferential sources for the metasediments (possibly granitic) rocks of 2100 Ma of age.

In order to constrain ages regarding the generation of tourmalinites, Brentan (2011) carried out U-Pb dating of detrital and volcanic zircon crystals by LA-ICP-MS at the Geochronological Research Center of the Geosciences Institute (São Paulo University). Because it was not possible to separate enough zircon crystals from the tourmalinites, zircon separates from rocks adjacent to the tourmalinites were used, such as garnet-biotite schist, calc-silicate and metabasic rocks (for more details on the separation method and zircon typology, see Brentan, 2011).

The zircon populations from the calc-silicate rocks yielded two very distinct Paleoproterozoic ages, the older of 2101 ± 16 Ma, corresponding to inherited nuclei and interpreted as the age of the igneous protolith formation, and the younger of 1956 ± 17 Ma, which corresponds to the Paleoproterozoic metamorphism that promoted a visible overgrowth on the igneous zircon crystals. A concordant age of 1784 Ma was also obtained for these rocks, which defines the oldest limit possible for the deposition of sediments that generated the calc-silicate rocks.

The garnet-biotite schist zircon crystals yielded four age groups. The oldest of 2152 ± 37 Ma is related to the source areas of the Brusque paleobasin detrital zircons. The second group yielded Mesoproterozoic age, which is equivalent to the Namaqua Metamorphic Complex zircon ages (Yamamoto, 2010). A younger age of 581 ± 40 Ma is related to the Brusque Group metamorphic peak and is very close to the ages of the post-metamorphic Brusque Group granitic intrusions (Basei et al., 2000, 2008, 2011; Silva et al., 2003).

Zircon crystals from the metabasic rocks yielded two age groups: 608 ± 10 Ma and 639 ± 11 Ma. The older age is probably related to that of the rock formation, whereas the younger to hydrothermal processes associated with granite emplacement and consequently to the Brusque Group thermal climax.

Another age of 591.7 ± 6.2 Ma yielded by zircons from the metabasic rocks may be related to the emplacement of the Valsungana batholith at 588 ± 6.2 Ma, the latter age obtained by Basei et al. (2011) with the SHRIMP method.

Because the tourmalinites overlie the metabasic rocks, whose oldest age is 639 ± 11 Ma, and taking into account that they underwent both deformation and metamorphism that took place in the Brusque Group, which is shown by the crenulation of the main foliation, the maximum age of tourmalinite formation is constrained to the 639 – 591 Ma interval.

MINERAL CHEMISTRY

Electron microprobe analyses (EPMA)

In situ electron microprobe analyses (EPMA) were performed at the Electron Microprobe Laboratory of the Geosciences Institute – São Paulo University (IGc/USP), equipped with a JXA-8600 JEOL Superprobe. Such equipment has five spectrometers, each one with two analyzers (STE/TAP, TAP/PET, PET/Lif, PET/Lif, PET/Lif), and runs by means of a Voyager 4.4 Thermo-Noran automation system. The instrument was operated at a beam diameter 1 – 2 μm, beam current 15 nA and acceleration voltage 15 kV. Carbon-coated, polished 80 μm-thick thin sections of tourmalinite samples IT-VI-42 (Rio do Oliveira) and IT-VII-39 (Morro do Carneiro) were used in the tourmaline analyses. When possible, color zones, cores and rims of individual tourmaline crystals were analyzed.

Structural formulae were calculated on the basis of 29 oxygen atoms per formula unit and assuming (i) 3 boron atoms per formula unit; (ii) T site filled with Si and Al up to 6 cations; (iii) Z site filled with Al and Fe (assumed as Fe^{3+}) up to 6 cations; (iv) Y site filled with Mg, Fe (assumed as Fe^{2+}), Mn, Cr, Ti, and any excess Si from (ii) and Al from (ii) and (iii); and (v) occupancy of the X site with Ca, Na and K. The analyses of 10 tourmaline crystals from Morro do Carneiro (labeled 39) and five from the Rio do Oliveira (labeled 42A) are listed in Table 1.

The tourmalines of the Rio do Oliveira tourmalinites fall in field 4 of Henry and Guidotti's (1985) Fe-Al-Mg diagram (Figure 5A), which is the field of tourmalines from metapelites and metapsammites coexisting with an Al-saturating phase. In the Ca/(Ca+Na) *versus* Mg# [= Mg/(Mg+Fe), atomic proportions] diagram of Figure 5B, the Rio do Oliveira tourmalines fall close to the dravite end-member. Except for one analysis (42A C8-N, Table 1), which corresponds to the core of tourmaline C8 and which is richer in FeO (7.14 wt.%, resulting in Mg# = 0.61) and poorer in CaO (0.07 wt.%) than the rim (Table 1, analysis 42A C8-B), there are no striking compositional differences between cores and rims of the Rio do Oliveira tourmalines. Relatively to

Table 1. Electron microprobe analysis of Morro do Carneiro (39) and Rio do Oliveira (42) tourmalines. Ions calculated on the basis of 31 oxygen atoms and 3 boron atoms.

Sample	39 C1-b	39 C1-i	39 C1-n	39 C2-b	39 C2-n	39 C3-b	39 C3-i	39 C3-n	39 C4-b	39 C4-n	39 C5-b	39 C5-n	39 C6a-b	39 C6a-i	39 C6a-n	39 C6b-b	39 C6b-n
SiO_2	36.44	35.85	35.84	36.68	36.04	36.65	36.62	35.94	36.26	36.42	36.76	36.14	36.47	35.60	35.88	36.65	36.67
TiO_2	0.80	1.25	1.12	0.62	0.67	0.88	0.66	0.87	0.47	0.78	0.60	0.52	0.68	1.11	0.74	0.69	0.55
Al_2O_3	30.40	29.94	30.59	30.43	32.44	29.94	30.18	29.32	30.69	31.12	30.04	32.12	29.63	30.01	33.44	30.09	30.40
Cr_2O_3	0.03	0.03	0.04	0.01	0.03	0.00	0.02	0.01	0.01	0.01	0.02	0.02	0.02	0.00	0.02	0.02	0.00
FeO	6.50	7.86	7.43	5.91	7.28	5.76	5.72	5.81	5.49	7.78	5.44	7.57	5.69	7.91	8.57	5.45	5.24
MnO	0.04	0.04	0.04	0.03	0.06	0.03	0.04	0.04	0.05	0.05	0.04	0.04	0.06	0.02	0.04	0.07	0.04
MgO	9.13	8.56	8.59	10.07	8.30	9.43	9.62	9.33	10.40	7.74	10.00	7.64	9.88	7.74	5.91	9.67	9.54
CaO	2.27	2.61	2.13	2.27	1.42	2.40	2.35	2.43	2.25	1.96	2.34	1.65	2.80	2.30	0.52	2.34	2.24
Na_2O	1.13	0.85	0.97	1.31	1.29	1.17	1.02	1.07	1.28	0.90	1.20	1.06	0.99	0.95	1.48	1.02	1.20
K_2O	0.02	0.02	0.03	0.03	0.02	0.02	0.03	0.03	0.02	0.01	0.03	0.01	0.03	0.02	0.01	0.05	0.02
F	0.47	0.26	0.29	0.30	0.38	0.30	0.01	0.30	0.43	0.42	0.13	0.09	0.82	0.05	0.50	0.26	0.00
Cl	0.02	0.03	0.00	0.01	0.04	0.00	0.01	0.00	0.00	0.01	0.02	0.00	0.00	0.00	0.01	0.00	0.00
Total	87.22	87.29	87.06	87.68	87.96	86.58	86.29	85.15	87.34	87.20	86.62	86.86	87.07	85.70	87.11	86.30	85.88
SiT	5.874	5.838	5.826	5.882	5.770	5.942	5.967	5.930	5.820	5.891	5.957	5.874	5.860	5.907	5.797	5.949	5.985
AlT	0.126	0.162	0.174	0.118	0.230	0.058	0.033	0.070	0.180	0.109	0.043	0.126	0.140	0.093	0.203	0.051	0.015
AlZ	5.651	5.586	5.688	5.635	5.892	5.665	5.764	5.635	5.626	5.825	5.696	6.000	5.473	5.778	6.000	5.707	5.833
SiY	0.000	0.000	0.000	0.000	0.000	0.000	0.000	0.000	0.000	0.000	0.000	0.000	0.000	0.000	0.000	0.000	0.000
AlY	0.000	0.000	0.000	0.000	0.000	0.000	0.000	0.000	0.000	0.000	0.000	0.028	0.000	0.000	0.167	0.000	0.000
Ti	0.097	0.153	0.137	0.074	0.081	0.108	0.081	0.108	0.057	0.095	0.073	0.064	0.082	0.138	0.090	0.084	0.067
Mg	2.194	2.078	2.080	2.407	1.981	2.278	2.337	2.295	2.487	1.866	2.416	1.851	2.367	1.913	1.423	2.339	2.321
Cr	0.003	0.004	0.005	0.002	0.004	0.000	0.002	0.001	0.001	0.001	0.002	0.002	0.002	0.000	0.003	0.003	0.000
Fe_2	0.528	0.657	0.699	0.426	0.866	0.445	0.545	0.437	0.363	0.877	0.432	1.028	0.237	0.876	1.492	0.447	0.548
Fe_3	0.348	0.414	0.312	0.365	0.108	0.336	0.235	0.365	0.374	0.175	0.305	0.000	0.528	0.222	0.000	0.292	0.167
Mn	0.005	0.006	0.006	0.004	0.008	0.004	0.005	0.006	0.007	0.007	0.006	0.006	0.008	0.002	0.005	0.009	0.005
Ca	0.392	0.456	0.37	0.391	0.243	0.417	0.411	0.429	0.386	0.339	0.406	0.288	0.482	0.41	0.09	0.406	0.392
Na	0.353	0.269	0.305	0.408	0.401	0.366	0.321	0.344	0.397	0.282	0.377	0.334	0.307	0.304	0.462	0.322	0.379
K	0.003	0.003	0.006	0.007	0.004	0.005	0.007	0.006	0.004	0.002	0.006	0.002	0.007	0.003	0.003	0.011	0.003
vacX	0.252	0.272	0.319	0.194	0.352	0.212	0.261	0.221	0.213	0.377	0.211	0.376	0.204	0.283	0.445	0.261	0.226
TotalCat	15.574	15.626	15.608	15.719	15.588	15.624	15.708	15.626	15.702	15.469	15.719	15.603	15.493	15.646	15.735	15.62	15.715
Mg#	0.71	0.66	0.67	0.75	0.67	0.74	0.75	0.74	0.77	0.64	0.77	0.64	0.76	0.64	0.55	0.76	0.76

Continues...

Table 1. Continued.

Sample	39 C7a-b	39 C7a-b2	39 C7b-br	39 C7b-i	39 C7b-n	39 C8-b	39 C8-n	42A C1-B	42A C1-N	42A C4-N	42A C5-N	42A C7inf	42A C7sup	42A C8-B	42A C8-N
SiO_2	37.21	36.92	36.87	35.87	36.66	37.09	36.61	37.25	36.89	37.10	36.92	36.91	36.57	36.60	36.64
TiO_2	0.69	0.54	0.11	1.04	0.24	0.53	0.58	0.38	0.39	0.25	0.29	0.50	0.28	0.31	0.57
Al_2O_3	30.28	30.19	31.86	30.77	32.32	30.24	33.65	33.30	33.14	34.56	33.36	31.81	33.78	32.76	33.08
Cr_2O_3	0.01	0.00	0.03	0.01	0.01	0.04	0.05	0.01	0.21	0.02	0.03	0.05	0.01	0.03	0.04
FeO	5.35	5.40	8.79	8.26	8.75	5.59	8.19	4.69	4.87	3.81	4.87	4.79	4.28	4.42	7.14
MnO	0.03	0.03	0.04	0.05	0.03	0.05	0.04	0.00	0.06	0.01	0.03	0.07	0.01	0.00	0.01
MgO	9.70	9.96	6.47	8.08	6.34	9.88	6.29	7.68	7.68	7.40	8.08	8.17	8.16	7.76	6.40
CaO	2.29	2.37	0.06	2.15	0.18	2.35	0.20	0.29	0.36	0.16	0.21	0.40	0.27	0.21	0.07
Na_2O	1.15	1.21	1.70	0.90	1.56	1.13	1.71	2.24	2.27	1.96	1.80	1.85	1.77	1.59	1.73
K_2O	0.03	0.03	0.03	0.02	0.02	0.03	0.03	0.00	0.00	0.00	0.00	0.00	0.00	0.00	0.00
F	0.47	0.26	0.04	0.59	0.09	0.25	0.30	0.25	0.02	0.09	0.04	0.47	0.43	0.26	0.22
Cl	0.02	0.01	0.00	0.00	0.00	0.02	0.02	0.01	0.00	0.00	0.00	0.02	0.00	0.03	0.01
Total	87.21	86.91	85.98	87.75	86.19	87.19	87.66	86.10	85.88	85.35	85.62	85.04	85.56	83.97	85.90
SiT	5.957	5.952	6.056	5.790	6.002	5.963	5.871	5.979	5.969	5.968	5.969	5.995	5.879	5.996	5.958
AlT	0.043	0.048	0.000	0.210	0.000	0.037	0.129	0.021	0.031	0.032	0.031	0.005	0.121	0.004	0.042
AlZ	5.671	5.690	6.170	5.644	6.000	5.694	6.233	6.280	6.290	6.523	6.328	6.085	6.280	6.324	6.301
SiY	0.000	0.000	0.000	0.000	0.002	0.000	0.000	0.000	0.000	0.000	0.000	0.000	0.000	0.000	0.000
AlY	0.000	0.000	0.170	0.000	0.000	0.000	0.233	0.280	0.290	0.523	0.328	0.085	0.280	0.324	0.301
Ti	0.083	0.065	0.013	0.126	0.030	0.064	0.070	0.046	0.047	0.030	0.035	0.062	0.034	0.038	0.070
Mg	2.314	2.393	1.584	1.944	1.547	2.368	1.503	1.837	1.853	1.775	1.947	1.977	1.955	1.896	1.551
Cr	0.001	0.000	0.004	0.001	0.002	0.005	0.006	0.002	0.026	0.002	0.003	0.006	0.001	0.004	0.005
Fe_2	0.387	0.417	1.207	0.759	1.197	0.445	1.098	0.630	0.658	0.513	0.659	0.650	0.576	0.605	0.972
Fe_3	0.329	0.310	0.000	0.356	0.000	0.306	0.000	0.000	0.000	0.000	0.000	0.000	0.000	0.000	0.000
Mn	0.004	0.004	0.006	0.007	0.004	0.007	0.005	0.000	0.008	0.001	0.005	0.009	0.001	0.000	0.001
Ca	0.393	0.409	0.01	0.372	0.031	0.404	0.035	0.049	0.063	0.028	0.036	0.07	0.046	0.037	0.012
Na	0.355	0.377	0.541	0.283	0.495	0.351	0.533	0.697	0.712	0.611	0.563	0.583	0.553	0.506	0.546
K	0.005	0.006	0.006	0.004	0.003	0.005	0.006	0.000	0.000	0.000	0.000	0.000	0.000	0.000	0.000
vacX	0.247	0.208	0.443	0.341	0.471	0.24	0.426	0.254	0.225	0.361	0.401	0.347	0.401	0.457	0.442
TotalCat	15.542	15.671	15.597	15.496	15.55	15.649	15.489	15.541	15.657	15.483	15.576	15.442	15.446	15.41	15.458
Mg#	0.76	0.77	0.57	0.64	0.56	0.76	0.58	0.74	0.74	0.78	0.75	0.75	0.77	0.76	0.61

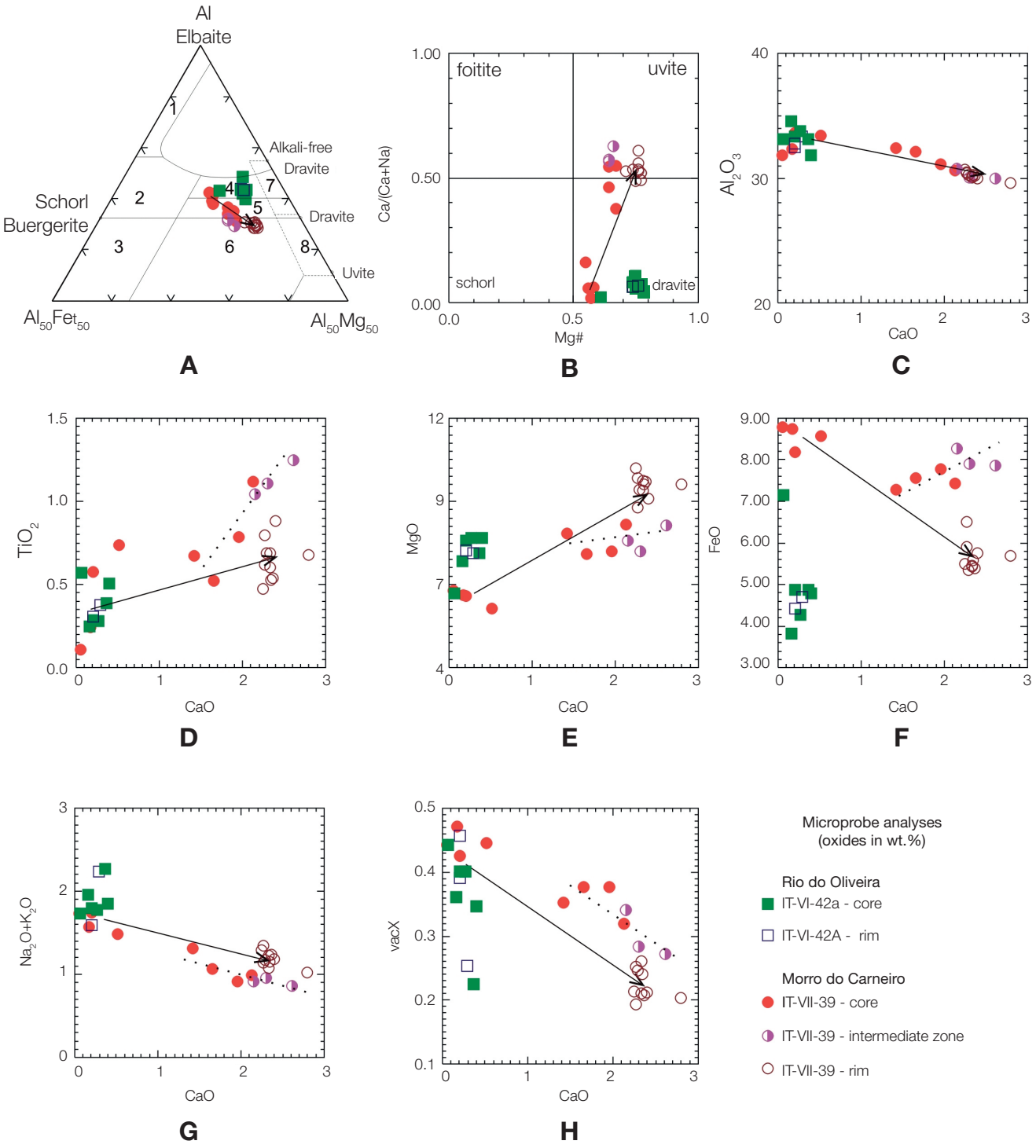

Figure 5. (A) Henry and Guidotti's (1985) Fe-Al-Mg diagram (atomic proportions). Numbered fields: 1. Li-rich granitoid pegmatites and aplites; 2. Li-poor granitoids and their associated pegmatites and aplites; 3. Fe^{3+}-rich quartz-tourmaline rocks (hydrothermally altered granites); 4. metapelites and metapsammites coexisting with an Al-saturating phase; 5. metapelites and metapsammites not coexisting with an Al-saturating phase; 6. Fe^{3+}-rich quartz-tourmaline rocks, calc-silicate rocks, and metapelites; 7. low-Ca metautramafics and Cr, V-rich metasediments; 8. metacarbonates and metapyroxenites. (B) Ca/(Ca+Na) *versus* Mg# (atomic proportions). (C to H) Major oxides (wt.%) and vacX (atomic proportions) *versus* CaO (wt.%). Arrows and doted lines: see text.

the Morro do Carneiro tourmalines, the Rio do Oliveira tourmalines are richer in Al_2O_3 (Figure 5C) and alkalis (Figure 5G) and poorer in TiO_2 (Figure 5D), MgO (Figure 5E), FeO (Figure 5F) and CaO. Except for two analyses, vacX > 0.34 (Figure 5H).

In contrast, Morro do Carneiro tourmalines predominantly fall in fields 5 and 6 of Henry and Guidotti's (1985) diagram, which are the fields of metapelites and metapsammites not coexisting with an Al-saturating phase and Fe^{3+}-rich quartz-tourmaline rocks, calc-silicate rocks, and metapelites, respectively (Figure 5A). CaO contents in the Morro do Carneiro tourmalines are higher than those of the Rio do Oliveira tourmalines, which in Figure 5B is indicated by compositions clustering around Ca/(Ca + Na) = 0.50 (atomic proportions).

The Morro do Carneiro tourmaline color zoning corresponds to an increase in MgO (Figure 5E) and decrease in FeO (Figure 5F), and alkalis contents (Figure 5G) from the light core to the greenish rim. There is an abrupt increase in CaO contents from core to rim, and even a "gap" between 0.52 and 1.42 wt.%. Because of the higher CaO contents at the rims, vacX < 0.26.

The intermediate (dark) zones of the Morro do Carneiro tourmalines (Figure 4D) are richer in TiO_2 and FeO and poorer in alkalis than the respective cores and rims, and there seems to be no relationship with the trends (arrows in Figure 5) defined by core and rim compositions.

It is interesting to note that the exceptional Rio do Oliveira tourmaline analysis 42A C8-N falls very close to the clusters of Morro do Carneiro tourmaline core compositions.

Laser ablation coupled to ICP-MS (LA-ICPMS) analyses

In situ trace-element analyses were performed by means of a New Wave UP-213 laser ablation system coupled to an Elan 6100DRC ICP-MS of the Chemistry and ICPMS Laboratory of the Geosciences Institute (São Paulo University). The carbon coating of the 80 mm-thick polished tourmalinite sections used in EPMA was removed, the sections were ultrasound cleaned and analyzed. Diameter crater varied from 40 to 55 mm when in spot mode and kept 30 mm at a 2 mm/s speed when in raster mode. Average time of analysis was 120 s. Reference materials used for calibration were synthetic glasses NIST SRM-610 and 612. The results were treated during each analysis by means of the Glitter 4.4.2 software for instrumental drift and fractionation corrections adopting NIST SRM-612 as internal standard. SiO_2 contents obtained by EPMA were used to adjust each analysis.

Tables 2 and 3 present the LA-ICPMS analyses respectively for the Rio do Oliveira and Morro do Carneiro tourmalines.

Due to the spot size, individual zones of either Rio do Oliveira or Morro do Carneiro tourmalines could not be analyzed. Even so, the LA-ICPMS analyses confirmed by the EPMA results in the sense that the Morro do Carneiro tourmalines are richer in Ti and Mg in relation to those of the Rio do Oliveira (Figures 6A and 6B). Additionally, they are also richer in Mn, Sr and Co (Figures 6C to 6E) and poorer in Cr (Figure 6F).

REE analyses, in particular those of Rio do Oliveira tourmalines, were very much influenced by the presence of zircon (see back-scattered electron image of Figure 8A), revealed not only by high Zr concentrations, but also by high Th, U, Y and HREE contents (Figures 6G to 6J).

Thanks to the Glitter 4.4.2 software, the effect of zircon in the tourmaline analyses could be estimated, as shown in Figure 7A, in which the REE patterns normalized to C1 chondrite values (Sun and McDonough, 1989) for zircon and tourmaline are represented.

Both Rio do Oliveira (Figure 7B) and Morro do Carneiro tourmalines (Figure 7C) are slightly enriched in La and Ce and depleted in the other REE elements in relation to C1 chondrite REE concentrations. In particular, HREE concentrations fall below detection limits.

Practically all REE patterns show positive Eu anomalies for tourmaline. Europium can exist as Eu^{2+} and may be fractionated from the other REE. As Eu^{2+}, it may directly substitute for other divalent cations, remarkably Ca^{2+}, whereas the other trivalent REE do not (Samson and Wood, 2005). Where this fractionation happens, the mineral formed is enriched in Eu relative to the other REE and will have a positive Eu anomaly.

DISCUSSION

Henry and Dutrow (1992) demonstrated the petrogenetic potential of tourmaline with the study of detrital tourmalines and their overgrowths from a chlorite-zone metawacke of the Devonian Temple Formation (Farmington Quadrangle, Maine – USA). By associating Ca, Ti and F contents obtained with the electron microprobe with Henry and Guidotti's (1985) Fe-Al-Mg diagram, these authors found a very wide range of compositions among different tourmaline grains and within a single grain that helped infer source rocks for the detrital tourmaline cores. In contrast to such compositional variability of the cores, the tourmaline overgrowths showed a remarkable consistency with

Table 2. Rio do Oliveira tourmalines: LA-ICPMS trace element concentrations and one-sigma errors for each analysis (values in ppm).

Sample	Turm1line	error	Turm1bspot40um	error	Turm2spot40um	error	Turm2bspot65um	error	Turm4line30um	error
Li_{7}	21.45	3.63	15.24	2.04	17.44	2.62	19.97	1.93	20.21	3.65
B_{10}	39591.75	20943.64	24020.03	13031.36	29635.85	16585.7	30021.15	17382.83	38331.45	23046.1
Mg_{25}	61220.79	8309.67	32602.64	4533.88	35122.67	5049.29	40973.09	6083.56	57151.99	8852.01
Si_{29}	170615.39	6073.68	170615.39	5654.24	170615.39	5795.24	170615.42	5460.22	170615.41	6102.68
P_{31}	< 54.44	38.13	< 49.97	27.53	< 47.86	27.98	< 9.97	5.13	< 56.15	38.89
Ca_{42}	1310.54	391.97	4068.51	390.92	2959.66	381.77	1528.65	128.17	2226.59	471.29
Sc_{45}	14.86	1.98	23.22	1.98	28.21	2.58	23.04	1.7	26.61	3.02
Ti_{49}	3529.76	994.26	3741.53	1094.56	2365.83	727.04	2901.74	934.01	5118.05	1742.37
V_{51}	118.95	11.4	71.95	6.93	90.35	9.12	98.61	10.01	129.68	14.36
Cr_{52}	168.92	14.18	74.37	6.73	81.38	7.89	73.21	6.05	179.09	17.33
Mn_{55}	98.32	12.24	169.28	21.05	183.54	23.91	124.17	16.75	242.79	34.9
Co_{59}	3.64	0.8	3.78	0.54	3.03	0.58	2.27	0.26	3.87	0.9
Ni_{60}	36.75	6.34	3.83	1.12	7.07	1.94	4.97	0.79	64.4	9.91
Cu_{65}	4.2	1.5	<0.66	0.48	< 0.70	0.38	0.52	0.18	4.75	1.72
Zn_{66}	61.9	12.78	43.81	8.42	30.09	6.84	21.64	4.17	82.59	18.25
Ga_{71}	38.48	9.51	17.69	4.43	29.28	7.54	34.39	8.9	34.34	9.59
Rb_{85}	< 0.154	0.048	< 0.152	0.059	0.14	0.11	< 0.027	0.019	< 0.192	0.06
Sr_{88}	102.19	25.32	88.48	22.42	68.22	17.87	57.41	15.51	99.47	28
Y_{89}	0.113	0.092	0.138	0.059	0.073	0.052	0.088	0.025	0.39	0.17
Zr_{90}	6.6	1.8	3	0.81	1.93	0.61	1.63	0.44	3.26	1.09
Nb_{93}	3.15	0.79	0.23	0.1	0.127	0.09	5.55	1.18	3.15	0.86
Mo_{95}	< 0.37	0.11	< 0.37	0.29	< 0.38	0.12	< 0.082	0.025	< 0.47	0.15
Cs_{133}	0.041	0.042	< 0.059	0.028	0.094	0.048	0.02	0.011	< 0.039	0.044
Ba_{137}	0.42	0.42	4.12	0.88	0.97	0.49	0.66	0.18	1.6	0.89
La_{139}	0.176	0.071	15.88	3.24	0.6	0.15	0.79	0.18	0.37	0.13
Ce_{140}	0.369	0.093	9.45	1.28	0.85	0.15	0.79	0.12	0.79	0.17
Pr_{141}	0.093	0.043	1.12	0.18	0.093	0.034	0.095	0.019	0.084	0.046
Nd_{143}	< 0.210	0.065	3.73	0.48	0.22	0.15	0.197	0.057	< 0.31	0.23
Sm_{147}	0.09	0.12	0.33	0.13	< 0.152	0.047	< 0.019	0.016	< 0.192	0.06
Eu_{151}	0.063	0.051	0.126	0.047	0.246	0.077	0.065	0.017	0.111	0.066
Gd_{155}	0.18	0.18	< 0.32	0.2	< 0.192	0.059	0.075	0.039	< 0.172	0.053
Tb_{159}	< 0.0148	0.005	< 0.030	0.018	< 0.022	0.014	< 0.0049	0.003	0.022	0.022
Dy_{163}	0.073	0.096	0.135	0.07	0.139	0.098	< 0.027	0.017	< 0.155	0.049
Ho_{165}	< 0.034	0.024	0.018	0.014	< 0.016	0.013	0.008	0.004	< 0.0207	0.006
Er_{166}	< 0.070	0.072	0.059	0.047	< 0.074	0.046	0.039	0.017	< 0.12	0.11
Tm_{169}	< 0.0260	0.008	< 0.034	0.015	< 0.00	< 0.00	0.006	0.003	0.021	0.021
Yb_{173}	0.11	0.15	0.053	0.053	0.34	0.18	< 0.042	0.019	< 0.245	0.078
Lu_{175}	< 0.0271	0.008	< 0.022	0.017	0.028	0.023	< 0.0073	0.004	< 0.0301	0.009
Hf_{179}	0.21	0.21	< 0.31	0.14	< 0.282	0.09	< 0.036	0.031	< 0.21	0.24
Ta_{181}	0.033	0.044	0.037	0.03	0.025	0.026	0.298	0.086	0.41	0.19
Pb_{208}	3.37	0.59	2.48	0.38	1.48	0.3	0.72	0.11	6.97	1.13
Th_{232}	1.79	0.53	1.84	0.46	9.54	2.23	0.218	0.064	0.3	0.17
U_{238}	0.3	0.13	0.099	0.045	0.105	0.057	0.06	0.02	0.27	0.13

Continues...

Table 2. Continued.

Sample	Turm4bspot40um	error	Turm5spot55um	error	Turm6spot55um	error	Turm7spot40um	error
Li_{7}	32.54	4.34	18.01	2.97	27.42	3.69	26.92	3.82
B_{10}	40011.66	24983.57	37099.69	28960.01	35989.39	29053.68	39479.72	32925.29
Mg_{25}	53123.9	8543.68	61892.7	12626.58	50215.79	10626.75	55055.22	12083.72
Si_{29}	170615.41	5849.62	170615.41	5757.47	170615.42	5532.55	170615.41	5564.15
P_{31}	< 55.03	31.02	99.27	34.75	< 30.40	13.55	< 36.72	16.54
Ca_{42}	1632.26	377.82	1622.07	267.11	2216.4	270.99	1571.09	257.05
Sc_{45}	32.1	3.13	27.21	3.06	33.24	3.44	85.24	8.89
Ti_{49}	4576.03	1643.99	4693.74	2379.17	4382.08	2350.53	3419.01	1941.17
V_{51}	138.89	15.79	132.13	20.11	157.72	25.02	192.77	32.16
Cr_{52}	155.45	15.29	123.72	15.7	118.19	15.35	167.22	22.63
Mn_{55}	179.75	27.06	144.36	29.56	154.38	33.1	164.48	37.08
Co_{59}	4.48	0.8	3.6	0.73	2.64	0.45	1.91	0.39
Ni_{60}	52.97	7.76	36.74	6.66	10.81	2.11	15.21	2.99
Cu_{65}	2.74	1.1	2.64	0.94	4.53	0.78	2.29	0.74
Zn_{66}	61.29	13.82	31.39	9.3	29.87	8.65	30.66	9.34
Ga_{71}	48.68	13.78	26.94	9.57	33.1	12.05	47.53	17.89
Rb_{85}	< 0.166	0.089	< 0.047	0.047	< 0.103	0.052	< 0.099	0.039
Sr_{88}	108.46	31.65	78.65	28.88	59.08	22.46	66.45	26.15
Y_{89}	1.43	0.31	0.161	0.078	0.094	0.041	0.142	0.056
Zr_{90}	47.14	13.05	5.11	1.85	1.51	0.57	0.96	0.39
Nb_{93}	9.92	2.36	1.76	0.58	0.56	0.19	0.86	0.3
Mo_{95}	< 0.75	0.24	< 0.00	< 0.00	< 0.27	0.15	0.32	0.2
Cs_{133}	< 0.051	0.03	0.037	0.031	< 0.051	0.021	< 0.047	0.027
Ba_{137}	0.54	0.38	0.17	0.22	0.78	0.27	0.47	0.22
La_{139}	0.56	0.16	0.38	0.14	0.96	0.33	0.46	0.17
Ce_{140}	0.73	0.15	0.6	0.15	1.12	0.26	0.66	0.16
Pr_{141}	0.077	0.034	0.027	0.016	0.11	0.032	0.083	0.028
Nd_{143}	0.81	0.29	0.24	0.16	0.37	0.12	0.105	0.076
Sm_{147}	< 0.18	0.12	< 0.102	0.069	0.09	0.055	0.081	0.048
Eu_{151}	0.096	0.055	0.097	0.051	0.07	0.029	0.059	0.025
Gd_{155}	< 0.23	0.14	0.19	0.13	< 0.180	0.065	0.17	0.1
Tb_{159}	< 0.019	0.015	< 0.00	< 0.00	< 0.0132	0.007	< 0.032	0.013
Dy_{163}	< 0.117	0.093	< 0.063	0.053	< 0.143	0.057	< 0.065	0.029
Ho_{165}	< 0.027	0.022	< 0.0151	0.005	< 0.0224	0.009	< 0.027	0.013
Er_{166}	< 0.107	0.086	0.037	0.039	< 0.083	0.035	< 0.070	0.028
Tm_{169}	0.027	0.019	< 0.018	0.012	< 0.0169	0.008	< 0.029	0.014
Yb_{173}	0.32	0.23	< 0.084	0.085	< 0.00	< 0.00	< 0.151	0.068
Lu_{175}	0.095	0.039	< 0.013	0.013	0.004	0.004	< 0.016	0.011
Hf_{179}	2.01	0.66	0.45	0.28	< 0.25	0.1	0.058	0.06
Ta_{181}	0.91	0.31	0.062	0.05	0.027	0.019	0.111	0.062
Pb_{208}	1.43	0.33	4.49	0.9	1.31	0.29	0.99	0.24
Th_{232}	0.7	0.25	2.59	0.88	0.5	0.19	0.49	0.19
U_{238}	0.57	0.19	0.121	0.065	0.079	0.038	0.032	0.021

Table 3. Morro do Carneiro tourmalines: LA-ICPMS trace element concentrations and one-sigma errors for each analysis (values in ppm).

Sample	TurmT1-2	error	TurmT1-2b	error	Turm4b	error
Li_{7}	33.41	8.32	13.3	3.51	45.7	9.33
B_{10}	37151.36	5047.82	18610.37	2618.99	28069.77	3277.38
Mg_{25}	80853.78	21970.31	35268.19	10161.21	54679.65	11325.1
Si_{29}	170615.36	5791.23	170615.34	5599.42	170615.36	5829.68
P_{31}	< 34.32	26.36	< 14.48	10.95	< 32.53	25.85
Ca_{42}	8953.72	1562.45	11649.46	2095.42	14984.13	1993.48
Sc_{45}	29.34	5.15	10.07	1.9	22.8	3.38
Ti_{49}	5981.26	1508.37	3455.65	918.37	6509.93	1286.37
V_{51}	82.24	10.24	77.65	****	145.5	14.36
Cr_{52}	169.09	14.35	< 1.66	1.29	214.01	14.95
Mn_{55}	238.31	42.69	236.94	44.82	242.58	33.49
Co_{59}	28.48	5.3	11.78	2.33	43.94	6.43
Ni_{60}	205.84	30.24	55.62	8.9	117.87	14.98
Cu_{65}	201.45	26.39	49.92	7.23	7.32	1.88
Zn_{66}	269.08	57.19	96.09	21.75	87.9	15.99
Ga_{71}	72.06	16.66	39.49	9.62	44.6	8.24
Rb_{85}	0.21	0.12	0.047	0.042	0.19	0.11
Sr_{88}	1274.43	413.58	689.94	237.53	2733.3	673.61
Y_{89}	0.41	0.18	0.017	0.022	0.23	0.11
Zr_{90}	8.85	1.78	0.56	0.19	0.9	0.31
Nb_{93}	0.48	0.19	0.17	0.079	0.39	0.17
Mo_{95}	0.64	0.47	< 0.100	0.032	< 0.303	0.095
Cs_{133}	0.093	0.052	0.082	0.037	0.027	0.027
Ba_{137}	4.65	1.17	1.02	0.39	0.22	0.28
La_{139}	1	0.21	0.249	0.062	2.85	0.44
Ce_{140}	3.66	0.89	0.44	0.12	3.74	0.71
Pr_{141}	0.14	0.049	0.018	0.012	0.401	0.094
Nd_{143}	0.067	0.089	0.19	0.1	1.57	0.42
Sm_{147}	< 0.095	0.03	0.031	0.039	< 0.075	0.089
Eu_{151}	0.31	0.11	0.163	0.057	0.76	0.19
Gd_{155}	0.25	0.18	< 0.00	<0.00	< 0.118	0.037
Tb_{159}	0.035	0.022	0.005	0.007	< 0.012	0.014
Dy_{163}	0.121	0.094	< 0.028	0.028	0.046	0.058
Ho_{165}	0.039	0.024	< 0.0081	0.007	< 0.0093	0.003
Er_{166}	0.031	0.041	< 0.0175	0.006	0.046	0.046
Tm_{169}	0.01	0.014	< 0.0071	0.007	< 0.0159	0.005
Yb_{173}	0.32	0.19	< 0.053	0.019	0.074	0.095
Lu_{175}	0.038	0.029	< 0.0042	0.001	< 0.0129	0.004
Hf_{179}	0.12	0.13	0.18	0.11	< 0.00	<0.00
Ta_{181}	0.062	0.04	0.08	0.032	0.254	0.085
Pb_{208}	8.77	1.34	2.48	0.42	5.36	0.77
Th_{232}	15.24	3.27	0.77	0.21	0.82	0.23
U_{238}	0.29	0.11	0.015	0.015	< 0.0196	0.006

Continues...

Table 3. Continued.

Sample	Turm4c	error	Turm5a	error	Turm5line	error	Turm6	error
Li_{7}	34.84	7.31	43.56	7.81	35.22	6.47	29.56	6.01
B_{10}	35529.75	4226.82	32691.2	3681.43	25346.59	2878.28	17485.9	2130.72
Mg_{25}	78041.71	16938.3	83491.27	16063.86	68253.13	13555.94	51405.81	11749.43
Si_{29}	170615.36	5716.16	170615.36	5472.22	170615.36	5471.73	170615.36	5453.39
P_{31}	< 23.15	17.85	< 32.58	14.18	< 22.95	11.24	< 21.61	9.68
Ca_{42}	18382.88	2514.56	22914.4	2733.03	15794.18	1948.5	11603.89	1643.97
Sc_{45}	16.87	2.58	28.9	3.61	16.31	2.12	12.79	1.86
Ti_{49}	4686.54	965.51	8153.97	1508.58	4411.11	838.28	3542.43	762.52
V_{51}	142.69	14.48	186.15	16.77	151.37	13.99	97.74	10.16
Cr_{52}	6.41	2.08	< 3.09	1.35	9.43	1.32	< 2.17	0.99
Mn_{55}	284.06	40.88	312.04	39.8	259.63	34.15	182.85	27.55
Co_{59}	21.45	3.34	21.56	2.86	17.11	2.34	12.68	1.96
Ni_{60}	107.76	13.78	118.64	12.61	87.15	9.6	59.76	7.39
Cu_{65}	< 0.171	0.053	0.96	0.29	1.76	0.39	1.39	0.33
Zn_{66}	147.35	26.06	139.55	21.25	126.2	19.8	102.58	18.28
Ga_{71}	63.21	11.91	74.49	12.35	61.84	10.56	44.79	8.7
Rb_{85}	0.084	0.073	< 0.045	0.022	< 0.049	0.027	0.073	0.038
Sr_{88}	870.99	225.22	970.94	222.2	625.79	147.91	520.65	141.9
Y_{89}	0.32	0.13	0.023	0.014	0.039	0.019	0.041	0.019
Zr_{90}	0.2	0.12	< 0.050	0.03	0.191	0.063	0.165	0.05
Nb_{93}	0.42	0.16	0.296	0.074	0.151	0.045	0.162	0.046
Mo_{95}	0.26	0.26	0.058	0.058	< 0.00	< 0.00	0.28	0.15
Cs_{133}	0.084	0.046	0.035	0.015	< 0.0172	0.007	0.025	0.012
Ba_{137}	2.02	0.67	2.26	0.36	1.69	0.3	1.23	0.24
La_{139}	0.244	0.061	0.342	0.052	0.217	0.036	0.216	0.038
Ce_{140}	0.374	0.092	0.478	0.086	0.268	0.052	0.361	0.076
Pr_{141}	0.019	0.015	0.046	0.013	0.046	0.012	0.026	0.008
Nd_{143}	0.16	0.12	< 0.121	0.063	0.086	0.042	0.075	0.035
Sm_{147}	< 0.050	0.064	< 0.070	0.033	< 0.032	0.018	< 0.046	0.021
Eu_{151}	0.24	0.079	0.231	0.048	0.2	0.044	0.134	0.032
Gd_{155}	0.067	0.082	< 0.126	0.044	< 0.072	0.023	< 0.042	0.028
Tb_{159}	0.017	0.014	< 0.0109	0.005	< 0.0051	0.003	< 0.0053	0.002
Dy_{163}	< 0.033	0.043	0.028	0.017	< 0.021	0.015	< 0.031	0.014
Ho_{165}	0.011	0.011	< 0.0087	0.006	< 0.0057	0.003	< 0.0099	0.005
Er_{166}	< 0.0188	0.006	< 0.037	0.016	< 0.025	0.013	< 0.025	0.013
Tm_{169}	< 0.011	0.011	< 0.0171	0.006	<0.0097	0.007	<0.0080	0.004
Yb_{173}	< 0.038	0.012	< 0.052	0.022	< 0.069	0.031	< 0.050	0.026
Lu_{175}	0.02	0.016	0.010	0.006	< 0.0096	0.005	< 0.0057	0.003
Hf_{179}	<0.10	0.1	0.068	0.04	< 0.089	0.036	0.053	0.031
Ta_{181}	< 0.015	0.019	0.051	0.019	0.048	0.015	0.036	0.011
Pb_{208}	4.58	0.65	4.69	0.52	4.66	0.53	3.24	0.41
Th_{232}	1.74	0.38	0.015	0.011	0.332	0.072	0.5	0.1
U_{238}	0.023	0.024	< 0.0179	0.008	0.021	0.011	< 0.0123	0.004

Continues...

Table 3. Continued.

Sample	Turm7b	error	Turm7b-2	error	Turm9	error	Turm10	error
Li_{7}	40.9	2.63	32.18	3.46	39.26	8.51	48.91	3.02
B_{10}	35391.29	5365.47	44874.97	7070.44	29634.09	3738.67	38705.17	5714.08
Mg_{25}	87834.23	18194.47	89535.13	19653.51	81142.48	19615.81	69051.71	13616.83
Si_{29}	170615.33	5500.13	170615.33	5739.31	170615.36	5565.62	170615.34	5509.82
P_{31}	< 53.91	23.9	< 57.14	38.06	< 35.45	18.72	< 27.43	15.25
Ca_{42}	18248.35	670.85	16832.96	787.7	18503.49	2783.08	17462.45	642.59
Sc_{45}	18.73	0.99	24.12	1.73	20.85	3.25	28.39	1.34
Ti_{49}	4840.54	1120.34	5451.01	1346.57	5372.64	1217.43	8525.15	1866.24
V_{51}	159.04	9.62	212.56	13.87	175.99	19.27	102.04	6.04
Cr_{52}	7.69	1.97	19.07	3.66	6.31	2.06	131.16	9.66
Mn_{55}	249.65	9.41	228.78	9.54	252.89	40.3	171.85	6.47
Co_{59}	19.07	1.57	15.92	1.69	21.05	3.47	58.22	4.3
Ni_{60}	112.91	10.63	77.04	9.11	146.39	19.1	140.75	12.6
Cu_{65}	2.09	0.52	4.26	1.28	8.76	1.54	7.34	1.07
Zn_{66}	117.66	15.51	98.82	15.1	123	23.48	65.44	8.51
Ga_{71}	65.76	8.51	72.36	10.22	75.16	15.44	34.44	4.31
Rb_{85}	0.118	0.061	< 0.128	0.091	< 0.111	0.059	1.07	0.13
Sr_{88}	813.87	50.18	674.09	44	1062.15	306.35	2739.1	162.14
Y_{89}	0.128	0.043	< 0.058	0.043	0.257	0.095	0.313	0.069
Zr_{90}	0.18	0.065	0.45	0.19	0.71	0.2	0.89	0.16
Nb_{93}	0.313	0.066	0.23	0.12	0.26	0.094	1.13	0.14
Mo_{95}	< 0.46	0.16	< 0.00	< 0.00	< 0.00	< 0.00	0.091	0.092
Cs_{133}	0.076	0.029	0.086	0.047	0.054	0.03	0.153	0.036
Ba_{137}	1.04	0.3	1.1	0.54	3.46	0.67	1.15	0.32
La_{139}	0.197	0.029	0.224	0.052	0.422	0.082	2.23	0.16
Ce_{140}	0.359	0.043	0.674	0.099	0.72	0.16	3.35	0.26
Pr_{141}	0.021	0.011	0.06	0.026	0.066	0.021	0.311	0.035
Nd_{143}	< 0.113	0.06	< 0.12	0.12	< 0.134	0.075	1.11	0.2
Sm_{147}	0.062	0.036	< 0.104	0.076	< 0.117	0.073	0.132	0.06
Eu_{151}	0.193	0.041	0.224	0.074	0.344	0.088	0.85	0.11
Gd_{155}	< 0.092	0.049	< 0.14	0.14	< 0.076	0.063	< 0.092	0.07
Tb_{159}	< 0.0158	0.008	0.023	0.016	< 0.0096	0.008	0.014	0.008
Dy_{163}	0.028	0.02	< 0.050	0.05	< 0.080	0.033	< 0.045	0.034
Ho_{165}	< 0.0160	0.007	0.02	0.017	0.006	0.006	< 0.0098	0.003
Er_{166}	0.043	0.022	< 0.086	0.045	0.065	0.042	0.012	0.012
Tm_{169}	< 0.0113	0.005	< 0.0171	0.005	< 0.023	0.011	< 0.0099	0.008
Yb_{173}	< 0.160	0.054	0.073	0.073	0.07	0.052	0.064	0.045
Lu_{175}	< 0.0121	0.008	< 0.0184	0.006	< 0.015	0.011	0.013	0.01
Hf_{179}	0.069	0.05	< 0.124	0.038	0.052	0.052	0.14	0.082
Ta_{181}	0.084	0.031	0.34	0.093	0.076	0.028	0.233	0.048
Pb_{208}	3.95	0.34	4.11	0.49	5.04	0.69	3.49	0.31
Th_{232}	0.07	0.027	5.93	0.56	1.16	0.26	2.45	0.21
U_{238}	< 0.0257	0.008	< 0.028	0.028	0.024	0.018	0.044	0.02

Continues...

Table 3. Continued.

Sample	Turm10b	error	Turm10c	error	Turm12a	error	TurmC-7a	error
Li_{7}	31.99	2.65	22.37	3.67	34.96	7.87	27.4	1.81
B_{10}	25476.71	4174.26	35568.91	6110.1	24579.74	3208.83	34880.25	5083.33
Mg_{25}	66165.72	15431.29	82793.65	20566.3	61947.3	15865.14	56565.87	10758.26
Si_{29}	170615.36	5558.98	170615.36	5989.2	170615.36	5515.15	170615.33	5478.46
P_{31}	< 28.63	18.43	< 37.92	40.83	< 25.12	12.94	< 45.17	20.16
Ca_{42}	11091.24	471.84	18185.22	950.05	9938.42	1587.14	1016.62	152.83
Sc_{45}	23.71	1.32	13.09	1.56	18.02	2.92	66.58	2.54
Ti_{49}	3614.32	953.4	3958.49	1121.07	2930.07	699.79	1748.99	367.72
V_{51}	157.78	10.59	180.93	13.5	113.14	13.02	361.4	20.18
Cr_{52}	4.92	1.59	9.28	3.26	< 2.63	1.39	49.87	3.91
Mn_{55}	198.1	8.06	260.73	12.02	216.83	36.53	100.32	3.76
Co_{59}	15.09	1.47	19.35	2.4	17.27	2.98	40.44	2.89
Ni_{60}	91.71	10.06	144.86	18.48	81.46	11.25	99.59	8.61
Cu_{65}	< 0.34	0.28	5.7	1.99	4.79	0.93	5.51	0.8
Zn_{66}	97.06	14.83	165.17	28.29	117.06	23.38	154.63	18.24
Ga_{71}	48.19	7.16	87.2	14.14	61.8	13.38	55.29	6.52
Rb_{85}	< 0.073	0.048	0.1	0.11	< 0.072	0.034	< 0.094	0.042
Sr_{88}	517.9	35.33	916.12	66.64	486.46	148.75	718.69	41.34
Y_{89}	0.055	0.032	< 0.0261	0.008	< 0.021	0.014	0.15	0.045
Zr_{90}	< 0.040	0.037	< 0.00	< 0.00	< 0.00	<0.00	0.185	0.06
Nb_{93}	0.239	0.072	0.16	0.11	0.121	0.052	0.362	0.07
Mo_{95}	< 0.146	0.045	<0.260	0.081	< 0.286	0.093	< 0.215	0.066
Cs_{133}	< 0.018	0.012	< 0.0158	0.005	< 0.013	0.011	< 0.037	0.018
Ba_{137}	0.56	0.26	0.37	0.43	1.29	0.33	0.61	0.19
La_{139}	0.104	0.024	0.232	0.071	0.123	0.031	0.155	0.022
Ce_{140}	0.19	0.035	1.75	0.24	0.157	0.042	0.198	0.026
Pr_{141}	0.016	0.009	0.032	0.023	< 0.0131	0.009	0.015	0.006
Nd_{143}	0.065	0.057	< 0.056	0.017	< 0.063	0.049	< 0.092	0.052
Sm_{147}	< 0.064	0.02	< 0.046	0.014	< 0.055	0.042	< 0.098	0.054
Eu_{151}	0.163	0.045	0.37	0.13	0.152	0.046	< 0.034	0.018
Gd_{155}	< 0.087	0.027	< 0.090	0.028	< 0.051	0.016	0.068	0.039
Tb_{159}	< 0.0122	0.007	< 0.00	< 0.00	< 0.0065	0.004	0.011	0.007
Dy_{163}	0.023	0.023	0.066	0.087	< 0.047	0.015	0.076	0.029
Ho_{165}	0.013	0.01	< 0.0112	0.004	< 0.0068	0.002	< 0.0130	0.007
Er_{166}	< 0.028	0.019	< 0.043	0.013	< 0.036	0.024	< 0.065	0.029
Tm_{169}	< 0.0106	0.003	< 0.0108	0.003	< 0.0153	0.008	< 0.0133	0.006
Yb_{173}	< 0.068	0.04	< 0.069	0.021	0.075	0.047	< 0.059	0.031
Lu_{175}	< 0.0115	0.009	< 0.0084	0.003	< 0.0121	0.004	< 0.0139	0.007
Hf_{179}	0.056	0.056	0.21	0.21	0.037	0.037	< 0.185	0.058
Ta_{181}	0.068	0.028	0.033	0.038	0.023	0.014	< 0.036	0.016
Pb_{208}	2.92	0.31	7.08	0.88	3.78	0.54	18.27	1.22
Th_{232}	< 0.0182	0.006	0.17	0.11	0.092	0.037	0.04	0.018
U_{238}	< 0.00	< 0.00	< 0.0178	0.006	< 0.0215	0.007	< 0.021	0.013

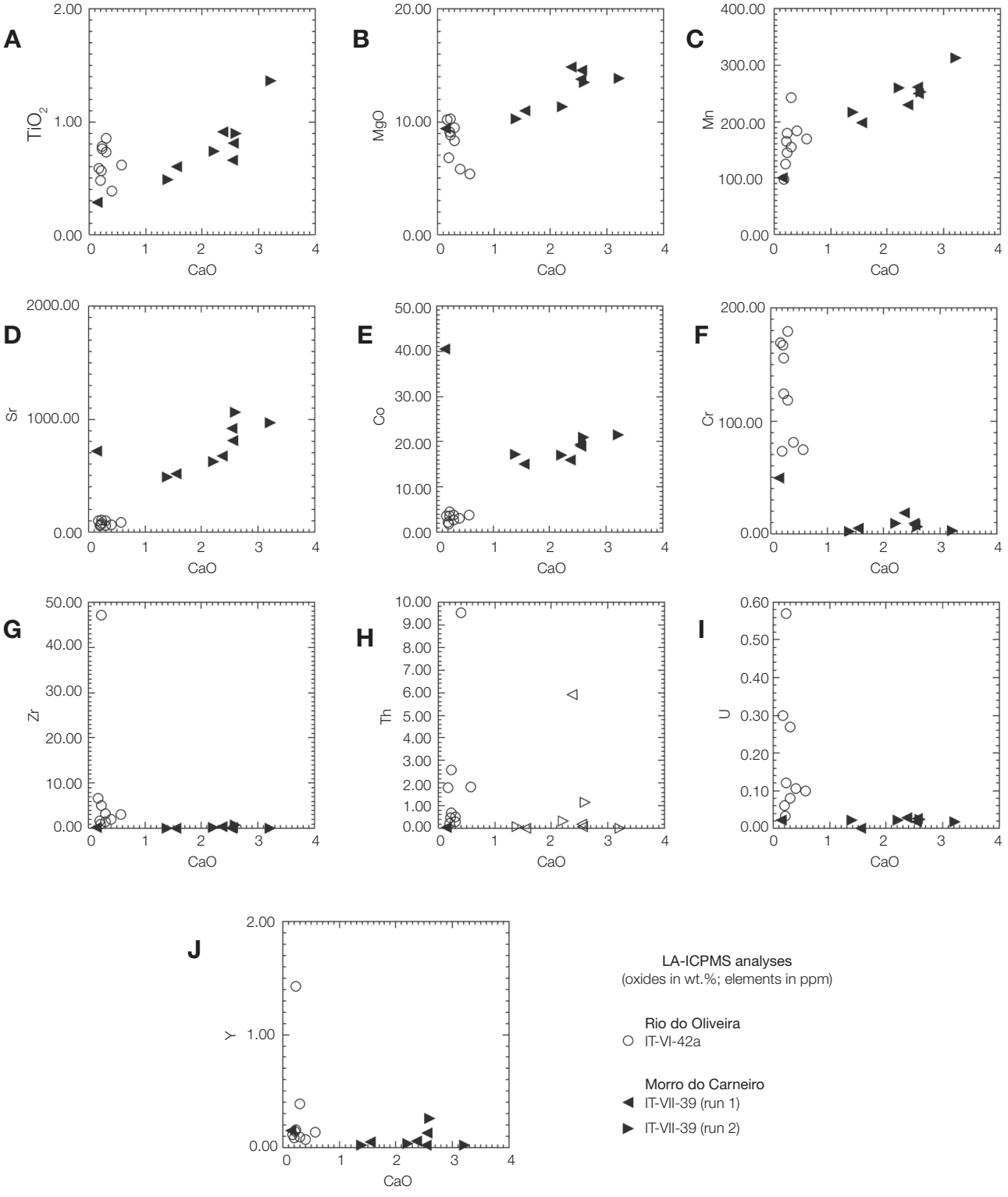

Figure 6. LA-ICPMS analyses. (A and B) TiO_2 and MgO (wt.%) *versus* CaO (wt.%). (C to J) Trace elements (in ppm) *versus* CaO (wt.%).

the metamorphic history of the area. Under low-grade metamorphic conditions, polar asymmetry can occur in growing tourmaline, so that the c^+ pole, which is usually paler, is enriched in Al and vacX compared to the darker c^- pole, enriched in Mg, Na, Ti and F.

The overgrowths of the Temple Formation tourmalines have an inner (proximal to the detrital tourmaline core) and an outer zone, which can be distinguished in back-scattered electron images and by abrupt Mg increase. The major change in composition from the inner to the outer zones is Mg substituting for Fe at both poles. Nonetheless, a substantial increase in F and Ca (at the expense of ^{Y}Al and vacX) occurs at the c^+ pole, whereas increase in Ca and ^{Y}Al (at the expense of Na and Ti) occurs at the c^- pole. Even the outermost rims of the tourmaline overgrowths displayed compositional polarity, being the c^+ pole enriched in ^{Y}Al, vacX and Si and depleted in Mg, Ca and Mg in relation to the c^- pole.

Compositional polarity diminishes with the increase in metamorphic grade and disappears in staurolite zone conditions. On the other hand, once polar asymmetry is established in tourmaline, it is not modified by subsequent metamorphism, even at higher grades (D. Henry, personal communication).

Back-scattered electron images of the Rio do Oliveira tourmalinite (*e.g.* Figure 8A) reveal that its tourmalines, despite the difficulty of observing zonation under the optical microscope due to grain size and color, are zoned. Semi-quantitative EDS analyses (not shown) indicate that there is increase in Na, Mg and Ca and decrease in Fe from cores to rims. Variable Ti and Al contents may reflect compositional polarity.

Based on Slack (1996) and associating the chemical variations of the Rio do Oliveira tourmalines with those of amphiboles from neighboring tourmaline-bearing schists, Brentan (2011) proposed that the Rio do Oliveira tourmalines were formed by selective substitution of pelitic and psammitic sediments, promoted by B-rich fluids percolating the Brusque paleobasin. According to Slack (1996.), the metasomatic formation of tourmaline in aluminous sediments involves the transformation of clay, mica, chlorite, and feldspar. Thus, sources of Si, Al, Fe, Mg, Ca and Na are available wholly from the local sediment, making the composition of the forming tourmaline similar to that of the host sediment. As for boron sources, besides submarine volcanic exhalations, Henry and Dutrow (1992) cite that boron adsorbed in clays can be released in significant amounts due to the change from 1M to $2M_1$ polytype during diagenesis and low grade metamorphism typically at 260 – 360ºC.

In turn, Morro do Carneiro tourmalines are color zoned, but the cores are not always composed of tourmaline. Figure 8B illustrates tourmaline overgrowing a quartz grain.

Figure 5 shows two groups of Morro do Carneiro tourmaline cores: one with compositions very similar to those of the Rio do Oliveira tourmalines (except for FeO), and the other with compositions defining a trend with those of the Morro do Carneiro tourmaline dark zones (represented with dotted lines in Figure 5). These two groups are separated by the CaO gap (0.52 wt.% < CaO < 1.42 wt.%).

It is possible that the first group (characterized by low CaO and high FeO contents) corresponds to detrital tourmalines, over which the dark zones and olive-green rims grew. Besides the abrupt increase in CaO and MgO contents, there is a sharp decrease in FeO,

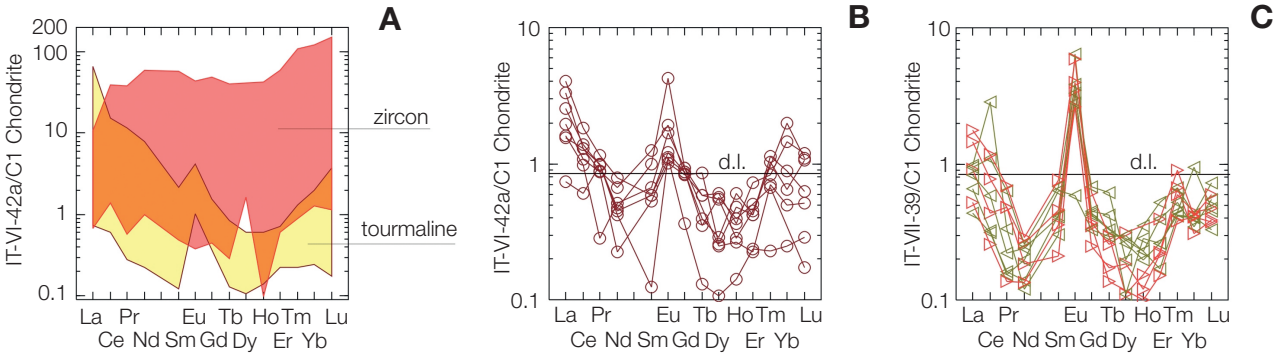

Figure 7. LA-ICPMS analyses (in ppm) normalized to C1 Chondrite (Sun and McDonough, 1989). (A) REE patterns for zircon and tourmaline from the Rio do Oliveira tourmalinite. (B) REE patterns for the Rio do Oliveira tourmalines. (C) REE patterns for the Morro do Carneiro tourmalines.

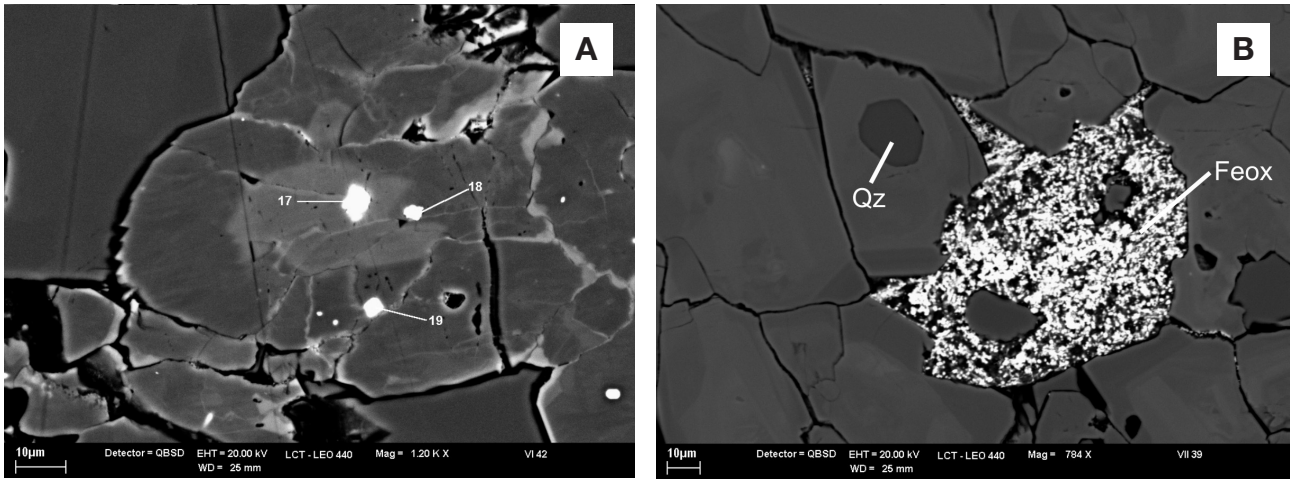

Figure 8. Back-scattered electron images. (A) Zircon crystals (numbered 17, 18 and 19) in the Rio do Oliveira tourmalinite. (B) Quartz core of a Morro do Carneiro tourmaline. Qz: quartz; Feox: iron oxides.

alkalis and vacX. According to Henry and Dutrow (1992), abrupt chemical discontinuities between zones implies that volume diffusion within tourmaline was minor under formation conditions.

Even considering the second core group (characterized by higher CaO, TiO_2 and MgO contents) as part of the trend defined by the dark zone or, alternatively, polar asymmetric in respect to the dark zone, compositional variations from this group to the olive-green rim are also sharp (increase in MgO and alkalis and decrease in TiO_2, FeO and vacX). Except for one analysis, CaO contents cluster around 2.3 wt.%, which indicates that the olive-rim reached equilibrium with the Ca-rich environment (underlying calc-silicate rocks).

CONCLUSIONS

The results obtained from the EPMA and LA-ICPMS analyses indicate that the Rio do Oliveira and the Morro do Carneiro tourmalinites were formed from fluids of distinct sources.

The Rio do Oliveira tourmalines are more Al-rich and may have been formed by selective substitution of pelitic and psammitic sediments promoted by B-rich exhalative fluids percolating the Brusque paleobasin. The Morro do Carneiro tourmalines, on the other hand, are richer in Ti, Fe, Mg, Mn, Sr, Co and specially Ca, and poorer in alkalis than the Rio do Oliveira tourmalines. The zoned tourmalines of the Morro do Carneiro tourmalinites show increase in Mg and Ca, and decrease in Al and Fe from core to rim. Increase in Ti and decrease in alkalis in the intermediate (dark) zone is also observed.

The sharp increase in CaO contents from core to rim of the Morro do Carneiro tourmalines may be explained by Ca input from the surrounding calc-silicate rocks.

The influence of metasomatic/igneous fluids is not ruled out, although REE patterns for the Rio do Oliveira and Morro do Carneiro tourmalines are practically identical. Such influence is attested by the younger (639 – 591 Ma) zircon populations in the tourmalinite adjacent rocks.

ACKNOWLEDGMENTS

The authors wish to thank FAPESP for previous (Procs. 05/56651-3, 05/58688-1, 06/06957-1 and 07/53895-4) and recent financial support (Proc. 2012/06687-5: *Turmalinitos do Grupo Brusque da região de São João Batista-Tijucas, leste de Santa Catarina – Brasil*) to the first author, allowing her participation in the 2012 Goldschmidt Conference in Poster Section 23D — General Geochemistry (Basei, Garda, Brentan, 2012). Our thanks for the invaluable assistance from Marcos Mansueto (probe analyses at the Electron Microprobe Laboratory, IGc-USP), Sandra Andrade (LA-ICPMS analyses at the Chemistry and ICP Laboratory, IGc-USP) the CPGeo team (zircon U-Pb dating), and Sheila Schuindt do Carmo (BSE images and EDS analyses at the Technological Characterization Laboratory, EP-USP). G.M. Garda also wish to thank Dr. Darrell Henry for fruitful discussion on tourmaline sector zoning and asymmetric nucleation during the Goldschmidt Conference in Montreal (Canada).

REFERENCES

BASEI, M. A. S. *O Cinturão Dom Feliciano em Santa Catarina*. 160 p., 1985. Thesis (Doctorate) – Instituto de Geociências, Universidade de São Paulo – USP, Brazil.

BASEI, M. A. S. *Geologia e modelagem geotectônica dos terrenos pré-cambrianos das regiões sul-oriental brasileira e uruguaia: possíveis correlações com províncias similares do sudoeste africano*. 123p, 2000. Associate Professor Monography – Instituto de Geociências, Universidade de São Paulo – USP, Brazil.

BASEI, M. A. S.; CAMPOS NETO, M. C.; SIGA JR., O. Geologia do Grupo Brusque na região de Canelinhas, SC. In: Congresso Brasileiro de Geologia, 38., 1994, Camburiú. *Extended Abstracts*... Camburiú: Sociedade Brasileira de Geologia; v. 1, p. 243-244, 1994.

BASEI, M. A. S.; SIGA JR., O.; MASQUELIN, H.; HARARA, O. M.; REIS NETO, J. M.; PRECIOZZI, F. The Dom Feliciano Belt of Brazil and Uruguay and its Foreland Domain the Rio de la Plata Craton: framework, tectonic evolution and correlation with similar provinces of Southwestern Africa. In: CORDANI, U. G.; MILANI, E. J.; THOMAZ FILHO, A; CAMPOS, D. A. *Tectonic Evolution of South America*, p. 311-334, 2000.

BASEI, M. A. S.; FRIMMEL, H. E.; NUTMAN, A. P.; PRECIOZZI, F. West Gondwana amalgamation based on detrital zircon ages from Neoproterozoic Ribeira and Dom Feliciano belts of South America and comparison with coeval sequences from SW Africa. *Geological Society Special Publication*, v. 294, p. 239-256, 2008.

BASEI, M. A. S.; CAMPOS NETO, M. C.; CASTRO, N. A.; NUTMAN, A. P.; WEMMER, K.; YAMAMOTO, M. T.; HUECK, M.; OSAKO, L.; SIGA JR, O.; PASSARELLI, C. R. Tectonic evolution of the Group Brusque, Dom Feliciano Belt, Santa Catarina, Southern Brazil. *Journal of South American Earth Sciences*, v. 32, p. 324-350, 2011.

BASEI, M. A. S.; GARDA, G. M.; BRENTAN, F. Tourmalinites of the Brusque Group in the São João Batista – Tijucas area, Santa Catarina State – Brazil. In: Goldschmidt Conference, 22. Montreal, Canadá. Electronic Abstract 1303, 2012.

BRENTAN, F. *Unidades turmaliníferas do Grupo Brusque, Rio do Oliveira, Tijucas, SC*. 41 p., 2011. (Graduation monograph) Instituto de Geociências, Universidade de São Paulo – USP, Brazil.

HARTMANN, L. A.; BITENCOURT, M. F.; SANTOS, J. O. S.; MCNAUGHTON, N. J.; RIVERA, C. B., BETIOLLO, L. Prolonged Paleoproterozoic magmatic participation in the Neoproterozoic Dom Feliciano Belt, Santa Catarina, Brazil, based on zircon U-Pb SHRIMP geochronology. *Journal of South American Earth Sciences*, v. 16, p. 477-492, 2003.

HENRY, D. J.; DUTROW, B. L. Tourmaline in a low grade clastic metasedimentary rock: an example of the petrogenetic potential of tourmaline. *Contributions to Mineralogy and Petrology*, v. 112, p. 203-218, 1992.

HENRY, D. J.; GUIDOTTI, C. V. Tourmaline as a petrogenetic indicator mineral: an example from the staurolite-grade metapelites of NW Maine. *American Mineralogist*, v. 70, p. 1-15, 1985.

PHILIPP, R. P.; MASSONNE, H. J.; THEYE, T.; CAMPOS, R. S. U-Th-Pb EMPA Geochronology of polygenetic monazites of the metapelitic migmatitic gneisses of Camburiu Complex, SC, Southern Brazil: evidences for the collisional and post-collisional events in Dom Feliciano Belt. In: Simpósio 45 Anos de Geocronologia no Brasil, 2004, São Paulo. *Boletim de Resumos Expandidos*, São Paulo, p. 289-291, 2004.

SAMSON, I. M.; WOOD, S. A. The rare earth elements: behaviour in hydrothermal fluids and concentration in hydrothermal mineral deposits, exclusive of alkaline settings. In: LINNEN, R.L.; SAMSON, I.M. (Eds.) Rare-element geochemistry and mineral deposits. *GAC Short Course Notes*, v. 17, p. 269-297, 2005.

SILVA, L. C. O Cinturão Metavulcanossedimentar Brusque e a evolução policíclica das faixas dobradas proterozóicas no sul do Brasil: Uuma revisão. *Revista Brasileira de Geociências*, v. 21, p. 60-73, 1991.

SILVA, L. C.; OLIVEIRA, J. M. P.; AUMOND, J. J.; LOPES, R. M. M.; EIPPER, J.; FERRO, G. Caracterização petrográfica da Sequência (Meta) Vulcano-sedimentar Rio do Oliveira (Cinturão do Itajaí Mirim, SC). In: Simpósio Sul-brasileiro de Geologia, 2, Florianópolis. *Atas*. Florianópolis: Sociedade Brasileira de Geologia, p. 11-23, 1985.

SILVA, L. C.; McNAUGHTON, N. J.; HARTMAN, L. A.; FLETCHER, I. R. Contrasting zircon growth patterns in Neoproterozoic granites in southern Brazil revealed by SHRIMP U-Pb analysis and SEM imaging: Consequences for the discrimination of emplacement and inheritance ages (preliminary approach). In: South America Symposium on Isotope Geology, 4., Salvador. *Proceedings*. Salvador, p. 687-690. 2003.

SUN, S.; McDONOUGH, W. F. Chemical and isotopic systematics of oceanic basalts: implications for mantle composition and processes. In: SAUDER, A. D.; NORRY, M. J. (Eds.) Magmatism in the ocean basins. *Geological Society of London Special Publication*, v. 42, p. 313-345, 1989.

SLACK, J. F. Tourmaline associations with hydrothermal ore deposits. In: GREW, E. S.; ANOVITZ, L. M. (Eds.) Boron – Mineralogy, Petrology and Geochemistry. *Reviews in Mineralogy*, v. 33, p. 559-643, 1996.

YAMAMOTO, M. T. *Geologia, proveniência e geoquímica isotópica da sequência metavulcanossedimentar do Grupo Brusque no Estado de Santa Catarina*. 39p, 2010. (Graduation monograph) Instituto de Geociências, Universidade de São Paulo – USP, Brazil.